HYDROLOGICAL PROCESSES
Hydrol. Process. **28**, 255–278 (2014)
Published online 5 November 2012 in Wiley Online Library
(wileyonlinelibrary.com) DOI: 10.1002/hyp.9568

Hydraulic subsurface measurements and hydrodynamic modelling as indicators for groundwater flow systems in the Rotondo granite, Central Alps (Switzerland)

U. S. Ofterdinger,[1]* Ph. Renard[2] and S. Loew[3]

[1] *Queen's University of Belfast, Environmental Engineering, David Keir Building, Stranmillis Rd., Belfast BT7 1NN, Northern Ireland*
[2] *University of Neuchâtel, Centre of Hydrogeology and Geothermics, 11 Rue Emile Argand, CH-2000 Neuchâtel, Switzerland*
[3] *ETH Zurich, Engineering Geology, Sonneggstrasse 5, CH-8092 Zurich, Switzerland*

Abstract:

Regional groundwater flow in high mountainous terrain is governed by a multitude of factors such as geology, topography, recharge conditions, structural elements such as fracturation and regional fault zones as well as man-made underground structures. By means of a numerical groundwater flow model, we consider the impact of deep underground tunnels and of an idealized major fault zone on the groundwater flow systems within the fractured Rotondo granite. The position of the free groundwater table as response to the above subsurface structures and, in particular, with regard to the influence of spatial distributed groundwater recharge rates is addressed. The model results show significant unsaturated zones below the mountain ridges in the study area with a thickness of up to several hundred metres. The subsurface galleries are shown to have a strong effect on the head distribution in the model domain, causing locally a reversal of natural head gradients. With respect to the position of the catchment areas to the tunnel and the corresponding type of recharge source for the tunnel inflows (i.e. glaciers or recent precipitation), as well as water table elevation, the influence of spatial distributed recharge rates is compared to uniform recharge rates. Water table elevations below the well exposed high-relief mountain ridges are observed to be more sensitive to changes in groundwater recharge rates and permeability than below ridges with less topographic relief. In the conceptual framework of the numerical simulations, the model fault zone has less influence on the groundwater table position, but more importantly acts as fast flow path for recharge from glaciated areas towards the subsurface galleries. This is in agreement with a previous study, where the imprint of glacial recharge was observed in the environmental isotope composition of groundwater sampled in the subsurface galleries. Copyright © 2012 John Wiley & Sons, Ltd.

KEY WORDS numerical modelling; alpine hydrogeology; fractured bedrock aquifers

Received 18 April 2011; Accepted 1 October 2012

INTRODUCTION

High alpine catchments in fractured crystalline rocks present a great challenge when assessing large scale groundwater flow systems. Regional flow systems are strongly influenced by topography and basin scale (Toth, 1963; Toth, 1984; Zijl, 1999; Winter, 2001; Gleeson and Manning, 2008). Furthermore, the geology (i.e. permeability and thermal conductivity), climatic conditions (available infiltration and surface temperatures) and regional heat flux are governing factors on regional flow systems (Forster and Smith, 1988a, b). Structural elements such as fault zones also strongly govern the behaviour of these systems (Forster and Evans, 1991; Lopez and Smith, 1995). Various conceptual approaches have been developed in the past decades to describe and model the groundwater flow through fractured rock masses (NRC, 1996) ranging from equivalent continuum models (Carrera *et al*., 1990; Bear, 1993) to discrete fracture network simulation models (Dverstorp and Andersson, 1989; Cacas *et al*., 1990a, b, c; Davy *et al*., 2006). Numerous case studies have been performed in fractured crystalline rock in the framework of the safety assessments for nuclear waste repositories (Kimmermeier *et al*., 1985; Herbert *et al*., 1991; Neretnieks, 1993) investigating flow and transport phenomena on the small scale and on a regional scale (Voborny *et al*., 1991; Voborny *et al*., 1994). Observations in subsurface galleries have been used to investigate groundwater flow systems within fractured crystalline rocks on a regional scale (Loew *et al*., 1996; Kitterod *et al*., 2000; Marechal and Etcheverry, 2003; Loew *et al*., 2007; Walton-Day and Poeter, 2009; Masset and Loew, 2010; Marechal, 2012). In high mountainous catchments, recharge conditions have strong spatial variability (Balek, 1988; Lerner *et al*., 1990; Kattelmann and Elder, 1991), depending on numerous factors such as geology/soil cover, topography/land form and vegetation/land use. The impact of varying recharge conditions and specific recharge sources such as snow pack and glaciers (Martinec *et al*., 1982; Manning and Solomon, 2005; Manning and Caine, 2007) in mountainous regions has been investigated mainly with the focus on shallow groundwater flow systems, and characteristic signatures

*Correspondence to: U.S. Ofterdinger, School of Planning, Architecture and Civil Engineering, Queen's University of Belfast, David Keir Building, Stranmillis Rd., Belfast BT9 5AG, Northern Ireland.
E-mail: U.Ofterdinger@qub.ac.uk

of recharge sources were shown in terms of environmental isotope content and hydrodynamic response (Flerchinger *et al*., 1992; Ward *et al*., 1999; Abbott *et al*., 2000; Hansmann *et al*., 2011).

To understand large scale groundwater flow systems in crystalline rocks of high mountainous terrain, a comprehensive study has been completed in the Rotondo Massif of the Central Swiss Alps. Various types of measurements were carried out at the terrain surface and in subsurface galleries. These range from the analysis of the hydrochemical and environmental isotope composition of groundwater and precipitation (Ofterdinger *et al*., 2004) to the acquisition of data on the structural geology and the measurement of hydrogeological parameters of the crystalline bedrocks. To improve our overall understanding of the groundwater systems, numerical simulations following a deterministic continuum approach were carried out. Spatially distributed recharge rates were extracted from the results of a hydrological model (Vitvar and Gurtz, 1999) and applied as upper boundary condition for the groundwater flow simulations.

Key questions addressed with the groundwater flow model are the influence of spatially distributed recharge on the groundwater flow field and the position of the free water table, the impact of subsurface galleries and the impact of a large scale fault zone on the regional flow system in this topographically complex terrain. The simulations are additionally aimed at providing a better understanding of the environmental isotope data and to test our previously derived interpretations of these (Ofterdinger *et al*., 2004). In the following, we first introduce the geological and hydrogeological setting of the study area. Then, the available information on hydrogeological parameters is illustrated, and our conceptual model is described before details of the modelling approach, and results are given. Concluding the discussion of the model results, a comparison with the findings from a previous study of the environmental isotope composition of the groundwater (Ofterdinger *et al*., 2004) in the study area is drawn.

GEOLOGICAL AND HYDROGEOLOGICAL SETTING

Major geological and hydrogeological units

The research area is situated in the western Gotthard-Massif of the Swiss Alps. Geologically, it consists mainly of the late Hercynian Rotondo granite and orthogneisses of early Palaeozoic age (Figure 1). The topographic elevation of the granite body ranges from 1800 to 3200 m a.s.l (Figure 2). On the northern margin of the study area, the Furka Tunnel passes through the granite body at an elevation of approx. 1490 m a.s.l. (Figure 1). An abandoned and unlined support segment to this base tunnel, the Bedretto Tunnel, is furthermore passing through the granite body in northwest-southeast direction. Due to the partial collapse of the Bedretto Tunnel, only the northern, approx. 1.5 km, are still accessible. Figure 2 shows, in particular, that this latter tunnel segment is also passing beneath glaciated areas of the study domain. It offers the opportunity for direct subsurface observations and was used for sampling of groundwater and monitoring of discharges and *in situ* parameters.

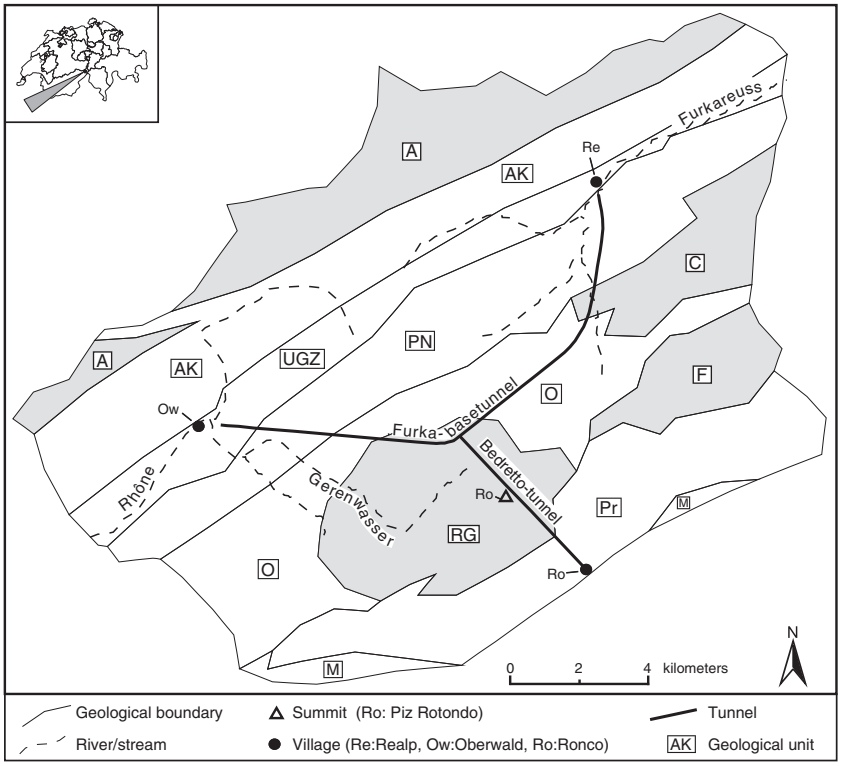

Figure 1. Schematic view of the model domain indicating the projected trace of the subsurface galleries and the individual geological units of the Aar-Massif and Gotthard-Massif (AM and GM) within the model domain [A, Aar-Granite (AM); AK, Southern Gneiss Zone (AM); UGZ, Urseren-Gavera Zone; PN, Northern Paragneis (GM); O, Orthogneiss (GM); Pr, Southern Paragneis (GM); M, Ultra-Helvetic Sediments (GM); RG, Rotondo Granite (GM); C, Cacciola Granite (GM); F, Fibbia Granite (GM)]

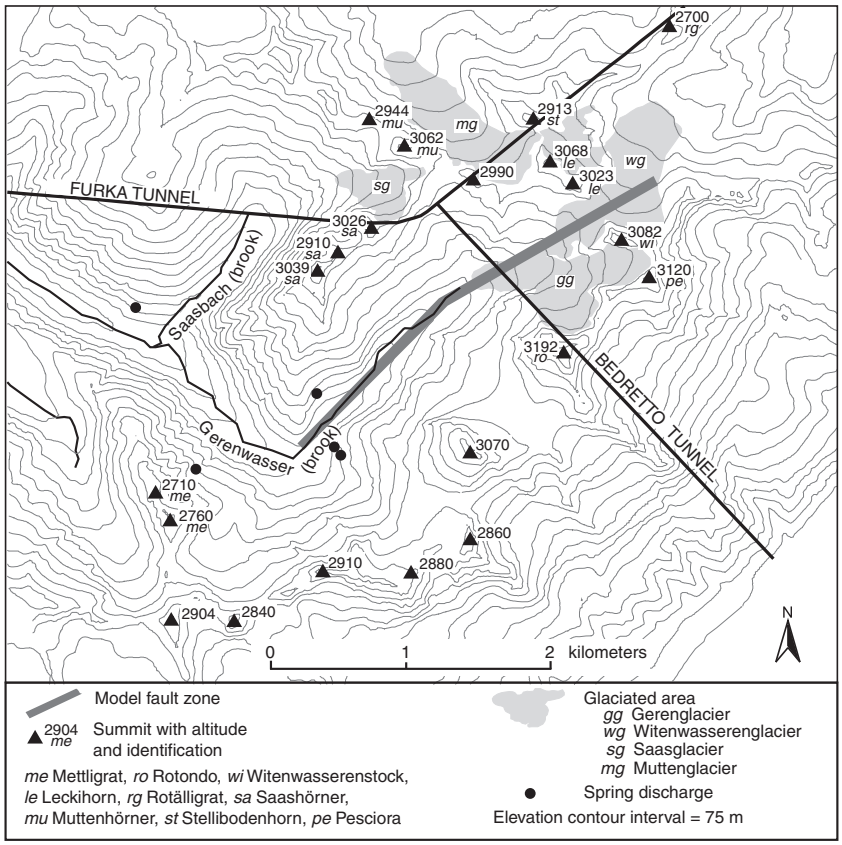

Figure 2. Enlarged plan view of the upper Gerental-valley in the model domain. Indicated are the projected tunnel trace together with the position of the glaciers, the location of mountain summits and the trace of the model fault zone intersecting the Bedretto Tunnel

The focus of this investigation is targeted on the groundwater flow systems within the granite body and its immediately adjacent formations. For the modelling purpose, the domain was however extended and includes additional geological units (Figure 1). From north to south, the geological units are the Hercynian Aar-Granite (A) and the Southern Gneiss Zone (AK) of the Aar-Massif. Between these units of the Aar-Massif and the units of the Gotthard-Massif to the south, the metamorphic sediments of the Permian-Jurrassic Urseren-Gavera-Zone (UGZ) can be found. Further to the south, the Cambrian-Palaeozoic Paragneisses (PN) and Orthogneisses (O) are followed by the Southern Paragneisses (Pr) within the Gotthard-Massif. Along the southern margin of the model domain follow the Triassic-Jurassic Ultra-Helvetic sediments (M) of the Gotthard-Massif. Additional to the Rotondo Granite, further Hercynian granite bodies can be distinguished within the domain. These are the Gamsboden/Cacciola-Granite (C) and the Fibbia-Granite (F). Throughout the area of the Gotthard-Massif and Aar-Massif, alpine faulting and foliation can be observed (Labhart, 1999; Zangerl *et al*., 2006; Luetzenkirchen and Loew, 2011). The former are often following pre-existing structures such as lithological boundaries, intrusive contacts or dykes and are found today mainly with steep to subvertical inclinations. Foliation is selective and less developed within the Variscian granites. These tectonic elements show mainly a NE–SW or E–W strike orientation with steep or subvertical inclination.

The geological boundaries indicated in Figure 1 are simplified for the modelling purpose and reflect the geological make-up of the domain on the massif-scale. The boundaries are extrapolated vertically with depth. The geological record of the Furka Tunnel and the Bedretto Tunnel (Keller and Schneider, 1982; Schneider, 1985b; Luetzenkirchen and Loew, 2011) show that for the Rotondo area, this simplification is valid because of the subvertical dip of the geological boundaries. Also in the rest of the model domain, mainly steep to subvertical lithological boundaries are observed (Labhart, 1999).

Structural geology

The Rotondo granite shows varying degrees of fracturation and faulting throughout the study area, changing both in lateral and vertical directions. Data on fracture orientation and fracture frequency (λ) were gathered by means of scanline surveys (Priest, 1993) on surface outcrops and along the unlined tunnel section of the Bedretto Tunnel. Twenty-three scanlines with lengths of 10–20 m were measured. Additionally, geological tunnel records (Schneider, 1985a) for the tunnel sections within the Rotondo granite as well as acoustic borehole televiewer data from a research borehole completed within the Rotondo granite were analysed leading to a database with 1174 fracture measurements. From this database, four major fracture sets can be deduced (Table I), where especially sets 1 and 2 are dominants at the ground surface. The NW–SE

Table I. Mean orientation of fracture sets with precision k and apical half-angle θ of 95%-confidence cone from Fisher analysis together with corresponding mean normal fracture frequency λ (and standard deviation σ; Priest 1993) from surface and tunnel outcrops

Number of set	Mean orientation	k	θ	$\lambda_{surface}$ (σ)	λ_{tunnel} (σ)
	strike/dip	[.]	[°]	[m^{-1}]	[m^{-1}]
1	049/75 SE	8.8	7.0	2.1 (2.2)	0.5 (0.2)
2	080/83 SE	16.5	5.0	1.5 (1.2)	0.2 (0.3)
3	140/86 SW	20.7	3.5	0.7 (0.6)	2.6 (2.7)
4	170/79 SW	7.4	5.8	0.04 (0.07)	0.3 (0.2)

striking fracture sets (3 and 4) are more abundant along the tunnel profile and are believed to be related to the tunnel construction, that is induced or reactivated by local stress amplifications. In addition to the steeply dipping sets described earlier, shallow dipping fractures can be identified at the terrain surface. These fractures generally strike subparallel to the valley axes with dip directions toward the valley bottom, most probably representing quaternary stress release joints. Occasionally, concentrical jointing can also be observed within the granite at ground surface. In addition to the fracturation, steeply dipping fault zones can be identified as important larger structural features, both at surface and along the tunnel profiles (Luetzenkirchen, 2002). The fault zones are mostly orientated subparallel or at acute angles to the general trend of the alpine structures of the Gotthard-Massif (ENE–WSW). It can be observed that both on the terrain surface and in the subsurface, specific fracture sets and sub-parallel orientated fault zones are the dominant water conducting features amongst the observed structural features (Ofterdinger, 2001; Luetzenkirchen, 2002).

One of the dominant steeply dipping fault zones in the research area is striking approx. 75° and follows the eastern part of the Gerental-valley (Figure 2) intersecting the Bedretto Tunnel in the subsurface, where it is associated with major groundwater inflows. Although the fault zone on the terrain surface is often obscured in the valley floor by scree deposits, it is consistently apparent through dense fracturation along the northwestern valley slopes and in the NW–SE trending mountain ridges to the east of the Bedretto Tunnel. In the subsurface, the structure of the fault zone can be directly studied along its intersection with the Bedretto Tunnel. Fault zones may be conceptually subdivided into fault core with fine-grained gouge material and adjacent fractured damage zone towards the surrounding protolith (Smith *et al.*, 1990b; Caine *et al.*, 1996). The observed approximately 120-m-wide zone, described in this paper, comprises several discrete fault zones of cm–dm width. Although the damage zones of these faults are pronounced and characterized by dense fracturation, only few lenses of fine-grained gouge material occur within these discrete faults. In the following, this 120-m-wide zone will be referred to as 'fault zone', in the conceptual context of this study, even though this term originally refers to an individual structure of the previously described succession of fault core, damage zone and protolith. For a detailed documentation of this zone and its structural elements, refer to Luetzenkirchen (2002), Luetzenkirchen and Loew (2001) and Luetzenkirchen and Loew (2011). Previous studies (Schneider, 1976) have traced this fault zone, which caused substantial problems during tunnel excavation (Keller and Schneider, 1982), on the surface along the Gerental valley and further to the east to an overall length of more than 10 km. As this interpretation is little constrained by direct observations (the fault zone to the east is obscured by glaciated areas and scree slopes), a conservative approximation of the modelled fault zone geometry was chosen with a length of approx. 4.5 km. The fault zone width was approximated to be constant with 120 m, although it is known that, generally, the width of fault zones may be highly variable and heterogeneous (Smith *et al.*, 1990b) both laterally and with depth. Yet, fault zones with similar widths at surface and in depth have also been observed (Raven, 1977; Wallace and Morris, 1979).

Environmental isotopes/hydrochemistry

In a previous study (Ofterdinger *et al.*, 2004), the composition of the groundwater from the Rotondo granite was studied with regard to environmental isotopes content and hydrochemistry. The analysis of the major ion chemistry and the $^{34}S/^{18}O$ content in aqueous SO_4^{2-} of sampled groundwater from the Bedretto Tunnel indicate that the encountered groundwater is derived primarily from within the granite body (Ofterdinger, 2001). A potential contribution from the northern neighbouring gneiss unit might serve as an explanation for an observed alignment of $^{34}S/^{18}O$-data along a mixing line with slope of approx. 0.6. Varying Ca/Na-ratios along the tunnel profile indicate the possibility of groundwater contributions from the neighbouring gneisses (O) and in particular from local amphibolite wedges.

The $\delta^{18}O$ measurements of groundwater samples underline their meteoric origin and indicate major contributions from accumulated winter precipitation to groundwater recharge. Especially along the previously described fault zone, tritium, $\delta^{18}O$ and temperature data imply a significant contribution of glacial melt water to groundwater recharge. Measured $\delta^{18}O$ reflect an altitude effect, that is higher recharge altitudes towards the northern end of the Bedretto Tunnel. Estimated recharge altitudes lie in the range of 2600–2800 m a.s.l. Along the whole Bedretto Tunnel, no indications for upwelling brines or convection driven flow are observed. Estimated mean residence times from lumped-parameter modelling of the $\delta^{18}O$-values in groundwater samples taken along the fault zone section are 1 to 1.5 years.

Spring line

Few obvious spring discharges from the granite bedrock can be observed in the Rotondo area. Their characteristic chemical composition is discussed in Ofterdinger *et al.* (2004). In the upper Gerental-valley, spring occurrences generally lie at an elevation of 2200–2300 m a.s.l, approximately 100–200 m above the valley floor (Figure 2). Even though these spring discharges were observed to originate from open fractures in the granite bedrock or associated to fault zones, the question whether the altitude of these springs truly marks the intersection of the water table with topography needs to be considered with caution, as near surface flow enhanced by shallow dipping stress-release joints in the decompressed zone might mask the true altitude of the water table along the slopes.

HYDROGEOLOGICAL PARAMETERS

Hydraulic heads

For the monitoring of hydraulic pressures within the Rotondo granite, a shallow dipping approx. 100-m-long research borehole was drilled from the tunnel gallery. The borehole is situated at the intersection of Furka Tunnel and Bedretto Tunnel below the Saashörner-ridge with an approximate overburden of 1200 m and a plunge direction of 165° (30° deviation from the axis of the Bedretto Tunnel). The orientation was chosen to intersect the observed prevailing water conducting steeply dipping fracture sets within the moderately fractured granite ($\lambda \sim 0.2$–$0.5\ m^{-1}$) at close to right angles. Two borehole intervals have been permanently packed by grout injection to monitor the hydraulic pressures. Monitoring intervals are 99.2–86.0 m (Interval 1) and 50.0–66.0 m (Interval 2) with perpendicular distances to the axis of the Bedretto Tunnel of approximately 43 and 29 m, respectively. Previously completed borehole fluid logging revealed inflows along these intervals of about 4 l/min (Interval 1) and 16 l/min (Interval 2) associated mainly with fractures of sets 1 and 2. Interval pressures are monitored via 1″ tubings at the borehole mouth. Monitoring started in July 1999. After a preliminary phase, the final sensor-setup with piezoresistive transmitters was installed in October 1999 (Type PA-53, Keller CH). Measured pressures are in the order of 50 bars for Interval 1 and 40 bars for Interval 2 (Figure 3). The recorded signal in Interval 1 shows annual fluctuations in the order of 1–1.5 bar with maximum pressures in November and minimum pressures in June. Whereas a similar pattern can be observed for 1999 in Interval 2, the pressure rise towards autumn 2000 is less clear. As calibration target for the individual intervals, the average hydraulic pressure measured for the period from 1 November 1999 to 1 November 2000 was chosen (Table VI). With respect to the modelling effort, these head measurements are not sufficient to fully constrain a regional model as they represent only a local area observation. Their purpose is mainly to investigate the long-term transient behaviour of a moderately fractured section of the Rotondo granite.

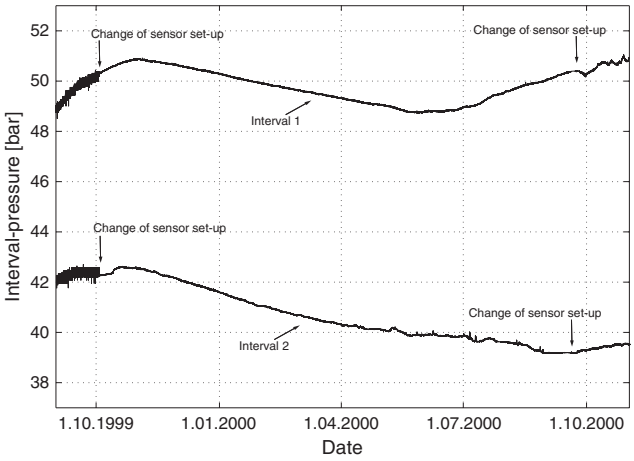

Figure 3. Long-term record of hydraulic pressures in the research borehole; data from monitoring intervals 1 and 2

Groundwater fluxes

Measurements of spatially integrated inflow rates to the subsurface galleries were carried out on a monthly/bimonthly basis. In the galleries, inflowing groundwater is captured in a basal drain and drained towards the tunnel portals. Inflows to the Furka Tunnel, east of kilometre BM11.4 (Figure 4), is drained towards the Realp-Portal whereas the remaining section is drained towards the Oberwald-Portal. No drainage water from the Furka Tunnel is passing through the Bedretto Tunnel. Groundwater inflows along this tunnel section are drained towards the southern Ronco-Portal. Measurements of integral flow rates along particular tunnel sections were carried out in the basal drain of the tunnels with depth-integrated velocity measurements (flow-anemometer). Discharge was then calculated according to ISO748:1997(E) (ISO, 1997). In the Furka Tunnel measurement, locations were chosen to characterize the inflow along the intersected section of the Rotondo granite as well as the total flow rates at the tunnel portals in Oberwald and Realp. In the Bedretto Tunnel, measurement locations were chosen to characterize the distribution of inflow rates along the tunnel profile and especially along the

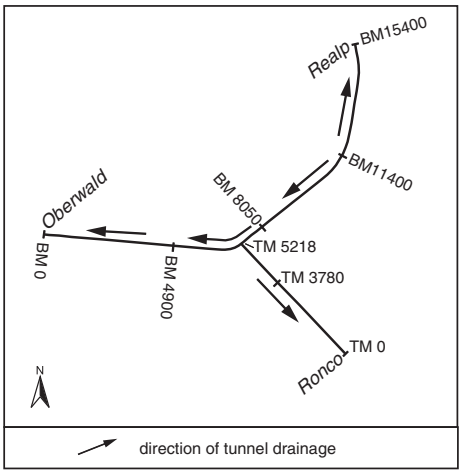

Figure 4. Schematic trace of the Furka Tunnel and Bedretto Tunnel. Indicated are the directions of the tunnel drainage and the tunnel metrics. Metrics refer to metre from the Oberwald-portal and Ronco-portal, respectively

intersected fault zone. Measurements were recorded from August 1998 to January 2000 in the Furka Tunnel and from November 1999 to November 2000 in the Bedretto Tunnel. Table II shows that the measured inflow rates show only small temporal variability, usually within the range of measurement errors.

Hydraulic conductivity

Several previous studies have been made to investigate the potential range of hydraulic conductivity of fractured crystalline rocks both on the laboratory as well as on the field scale (Brace, 1980; Brace, 1984; Clauser, 1992) and, in particular, the permeability distribution within fault zones and their adjacent crystalline formations (Davison and Kozak, 1988; Forster *et al*., 1994; Scholz and Anders, 1994; Evans *et al*., 1997; Caine and Forster, 1999; Masset and Loew, 2010). Commonly, a wide range of values are found spanning several orders of magnitude depending on the degree of deformation and the sampling position within the fault zone or neighbouring crystalline rock. Accordingly, a range of anisotropy ratios for fault zones are stated, describing the oftentimes observed enhanced fault-parallel flow in contrast to reduced fault-normal flow (e.g. Winkler *et al*., 2010).

A first approximation of the hydraulic conductivities of the more intact sections of the Rotondo granite was deduced from hydraulic tests completed in the research borehole (constant-rate tests). Four packer tests with increasing test interval length (7–35.5 m) were carried out starting from the bottom of the borehole. Apparent hydraulic conductivities (referenced to interval length) range from 6.0×10^{-9} to 2.9×10^{-8} m/s with a geometric mean of $1. \times 10^{-8}$ m/s.

On the basis of the measured inflow rates to the Bedretto Tunnel and assuming steady-state conditions, hydraulic conductivities for the fault zone section and the remaining granite section along the tunnel profile as well as for the whole profile length were approximated using the analytical solution described by Goodman (1965) on the basis of the assumption of a linear constant head boundary:

$$Q_0 = \frac{2\pi T H_0}{\ln\left(\frac{2H_0}{r}\right)} \quad (1)$$

with Q_0 being the discharge rate along the investigated section (m^3/s), T is the hydraulic transmissivity (m^2/s), H_0, the piezometric level above gallery (m) and r, the radius of gallery (m). Hydraulic conductivity k is then estimated from $T = k \times e$, with e being the width of the investigated zone (m). A range of potential hydraulic conductivities was calculated for fixed heads at the topographic surface (z) and at a piezometric level of $0.7z$. The latter assumption is based on observations in similar rock types and overburden within the scope of the Gotthard-base tunnel project of AlpTransit/NEAT in Switzerland (Koella, 1993). Table III summarizes the estimated values.

Within the scope of the AlpTransit/NEAT project (Loew *et al*., 2000), a comprehensive database of effective hydraulic parameters from the geological units of the Aar and Gotthard Massif has been compiled (Colenco, 1993; Masset and Loew, 2010). The derivation of effective transmissivities was thereby based on the observation of discharge rates to numerous existing tunnels and subsurface galleries in these formations (Loew *et al*., 1996). With these, effective hydraulic conductivities were calculated for longer tunnel sections (>100 m; Voborny *et al*. (1994)). The so derived hydraulic conductivity for Hercynian granites in the Gotthard Massif such as the Rotondo Granite at the tunnel elevation is 1.1×10^{-8} m/s. As no direct observational data was available in the scope of this study to constrain the hydraulic conductivities of the neighbouring geological units to the Rotondo granite, the mentioned database (Colenco, 1993) was used to establish initial approximations for the numerical model (Table IV).

Several studies have shown the depth-dependence of the hydraulic conductivity/transmissivity in crystalline rocks (Snow, 1968; Herbert *et al*., 1991; Thury *et al*., 1994; Manning and Caine, 2007; Masset and Loew, 2010; Marechal, 2012). Furthermore, it can be observed that a distinct hydraulic discontinuity occurs in the uppermost 100–200 m. Close to the terrain surface, substantially higher conductivities due to denser fracturation and larger apertures occur. This can be explained by stress release, weathering processes and gravitationally induced weakening of the

Table II. Mean measured integral flow rate to the accessible section of the Bedretto Tunnel (total) and to the fault zone section within the Bedretto Tunnel together with integral flow rate to the Rotondo Granite section of the Furka Tunnel as well as to the whole Furka Tunnel (measured at the Portals). Tabulated further are standard deviation σ as indicator for variability over time and associated error of the measurement. For tunnel metrics refer to Figure 4

Tunnel section	Tunnel metrics	Q	σ	Measurement error
	[m]	[l/s]	[l/s]	[l/s]
Bedretto Tunnel	TM3780-5218	14.9	0.3	±0.5
Fault Zone	TM4200-4320	7.5	0.1	±0.5
Furka Tunnel (RG)	BM4900-8050	25.8	1.2	±5.6
Portal Oberwald	BM0-11400	94.4	1.7	±5.9
Portal Realp[†]	BM11400-15400	75.8	0.1	±5.9

[†] Only four measurements November 1998–March 1999.

Table III. Analytical approximations of hydraulic conductivities. Values are calculated for the fault zone section and the remaining granite section as well as for the total tunnel section including the fault zone section

Section of Bedretto Tunnel	Hydraulic conductivity
	[m/s]
Fault zone	$6.0–8.2 \times 10^{-8}$
Remaining tunnel section	$6.0–8.3 \times 10^{-9}$
Total tunnel section	$1.0–1.4 \times 10^{-8}$

Table IV. Initial approximations of effective hydraulic conductivities (HC) for the geological units within the model domain together with calibrated HCfor the individual scenarios

Name	Index	Initial HC	Calibrated HC [m/s]		
		[m/s]	Scenario 1	Scenario 2	Scenario 3
Rotondo Granite	RG	1.1×10^{-8}	1.2×10^{-8}	6.0×10^{-9}	6.5×10^{-9}
Aar Granite	A	3.8×10^{-9}	nc	nc	nc
s' Aar Gneiss Zone	AK	5.3×10^{-9}	nc	nc	nc
Urseren-Gavera-Zone	UGZ	1.5×10^{-8}	nc	nc	nc
n' Paragneiss	PN	3.1×10^{-8}	3.1×10^{-9}	3.1×10^{-9}	3.1×10^{-9}
Orthogneiss	O	2.3×10^{-8}	9.2×10^{-9}	1.4×10^{-8}	1.4×10^{-8}
s' paragneiss	P	3.1×10^{-8}	nc	nc	nc
Ultra-Helvetic Sediments	M	4.0×10^{-7}	nc	nc	nc
Fibbia Granite	F	1.1×10^{-8}	nc	nc	nc
Cacciola Granite	C	1.1×10^{-8}	8.0×10^{-8}	8.0×10^{-8}	8.0×10^{-8}
Fault Zone	FZ	1.2×10^{-7}	—	6.0×10^{-8}	6.5×10^{-8}

HC, hydraulic conductivities; nc, no change; s', southern; n', northern.

bedrock along steep slopes. This zone if often referred to as the decompressed zone (Jamier, 1975; Raven, 1977; Cruchet, 1985; Marechal and Etcheverry, 2003) and can also be observed in the research area (Ofterdinger, 2001). On the basis of a review of studies in the crystalline rocks of the Swiss Alps and the crystalline basement of Switzerland, Marechal (1998) proposes an exponential decrease of hydraulic conductivity, where k (m/s) at a given overburden C (m) follows:

$$k = k_0{}^{\times e^{-a \times C}} \quad (2)$$

with k_0 being the hydraulic conductivity at surface. Marechal (1998) derives a value of $0.05\,m^{-1}$ for the exponent a for the uppermost decompressed zone, and a value of $0.005\,m^{-1}$ at depth. This approach has been adopted in this study, defining the decompressed zone as the uppermost 100 m of the massif. Although the depth dependence is frequently observed for the gneiss-formations within the Aar-massif and Gotthard-massif, this clear dependence is not observed within the Hercynian granites such as the Rotondo, Fibbia and Cacciola/Gamsboden granite (Colenco, 1993; Loew *et al.*, 1996; Masset and Loew, 2010). Furthermore, it can be observed that major water conducting faults often lack this depth-dependence (Thury *et al.*, 1994). Therefore, the hydraulic conductivity for the Hercynian granites was not modified with depth, except the distinction between the decompressed zone and the deeper subsurface.

The preferred orientation of fractures and faults, associated with inflows to the tunnel within the Rotondo granite and the pronounced structural anisotropy within the neighbouring gneisses (foliation) imparts an anisotropy on the hydraulic conductivity of these formations, promoting flow along the strike of these features. As their orientation is approximately subparallel or at acute angles to the overall strike of the Gotthard Massif, the anisotropy is simplified to be orientated globally with $k_1 > k_2$, whereby k_1 is orientated parallel to the overall strike of the massif (72°). As the structural features, such as the observed water conducting fractures within the granite, as well as the foliation in the gneisses are steeply subvertically inclined, the vertical component of hydraulic conductivity was set equal to the maximum horizontal component. Studies in similar rock types suggest anisotropy ratios in the range of $1 \leq 10$–170 (Hsieh *et al.*, 1985; Raven, 1985; Nagra, 1988). In the absence of further constrains on the absolute value of the anisotropy ratio, a conservative approximation of a 1:10 ratio was adopted for the numerical model.

Table III shows that the analytical approximation of the k-value for the fault zone is approximately one order of magnitude larger than the k-value approximated for the remaining tunnel section. Other studies have stated permeability contrasts between fault zone and neighbouring bedrock to be in the range of up to three orders of magnitude (Smith *et al.*, 1990b; Forster *et al.*, 1994; Caine *et al.*, 1996). However, most of these studies consider narrow discrete fault zones composed of the succession of fault gouge, damage zone and undamaged protolith. As stated earlier in this study, the term fault zone is attributed to a 120-m-wide zone comprising several narrow discrete faults with sections of densely fractured rock in between. Because of this, the contrast to the surrounding bedrock is expected to be less pronounced, compared to studies where a specific element of a discrete fault zone in the strict sense, for example, the damage zone, is compared with the essentially unfractured bedrock. Therefore, a conductivity contrast of 1:10 is initially set between the Rotondo granite as such and the fault zone within the granite. A similar contrast has been found by Colenco (1993) and Masset (2011) and has been applied in another study by Herbert *et al.* (1991) for a regional model.

Anisotropy within the fault zone is set to be $k_1 > k_2$, whereby k_1 is aligned parallel to the strike of the fault zone. Similar to the granite bedrock, the vertical component of hydraulic conductivity (k_3) was set to $k_3 = k_1$, as the fault zone is subvertically inclined. Many studies have shown the decreased fault-normal flow across fault zones, mainly caused by the low permeable central fault gouge and also by the preferred fault-parallel

orientation of fracturation within the adjacent damage zone (Smith *et al*., 1990b; Caine *et al*., 1996; Lopez and Smith, 1996). This anisotropy ratio has been shown to range between ≤10 (Andersson *et al*., 1991; Forster and Evans, 1991) up to several orders of magnitude (Smith *et al*., 1990b; Evans *et al*., 1997). As the fault zone in our case includes only very few gouge material, which would potentially inhibit fault-normal flow, an anisotropy ratio within the fault zone of 1:10 was initially assumed.

Groundwater recharge rates

Depending on topography, land use, vegetation and slope exposition, groundwater recharge shows strong variability across catchments (e.g. Lerner *et al*., 1990; Scanlon *et al*., 2002; Heppner *et al*., 2007). As the research area is situated in a high mountainous area covering a wide range of elevation zones, the spatial discretization of the groundwater recharge rates is a crucial factor for estimating the upper boundary condition of the groundwater flow model. For this reason, the recharge rates applied in the groundwater flow model were extracted from the results of a calibrated hydrological model of the study catchment.

The applied GIS-based model precipitation-runoff-evapotranspiration-hydrotope model combines the spatial differentiation of hydrologically similar response units or 'hydrotopes' and a runoff generation concept that allows the separate calculation of the water balance within each hydrotope (Gurtz *et al*., 1999; Viviroli *et al*., 2009). The hydrotopes were defined to represent hydrologically homogeneous areas according to the most important factors controlling evapotranspiration and runoff formation process, such as the meteorological inputs, topography (catchment area, altitude, exposition and slope), land use and soil characteristics (Gurtz *et al*., 1990). For the glaciated areas, a conceptual model was applied, which was developed for a research study in the Rhône area (Badoux, 1999). This concept attributes melt water from the glaciated areas below the equilibrium line preferentially to the fast runoff storage, whereas melt water originating above the equilibrium line preferentially contributes to the slow runoff storage, that is to groundwater recharge.

The hydrological model was first calibrated and validated in the area of main interest, the Gerental basin (approx. 40 km^2), and then applied to the larger groundwater flow model domain using identical model parameters as calibrated in the Gerental basin. The hydrograph simulation for the gauging station at the Gerental catchment outlet was performed for the period from January 1991 to October 1999. The results of the hydrograph simulation are discussed elsewhere (Vitvar and Gurtz, 1999). The temporal variations of the simulated recharge rates show maximum recharge rates in the upper Gerental-valley during spring and summer (April–September), commencing with the onset of the melting period.

The resulting recharge distribution shows a strong spatial variability, especially in the high altitude regions of steep bare rock slopes, where low recharge areas contrast to the upper regions of the glaciers, characterized by high recharge rates within small restricted areas (Figure 5 and 6). Another striking feature in the recharge distribution is the observation of low to moderate recharge rates along the valley floor and the lower valley slopes. From a hydrodynamic perspective, these areas are expected to constitute potential exfiltration areas, where essentially, no groundwater recharge should occur. This

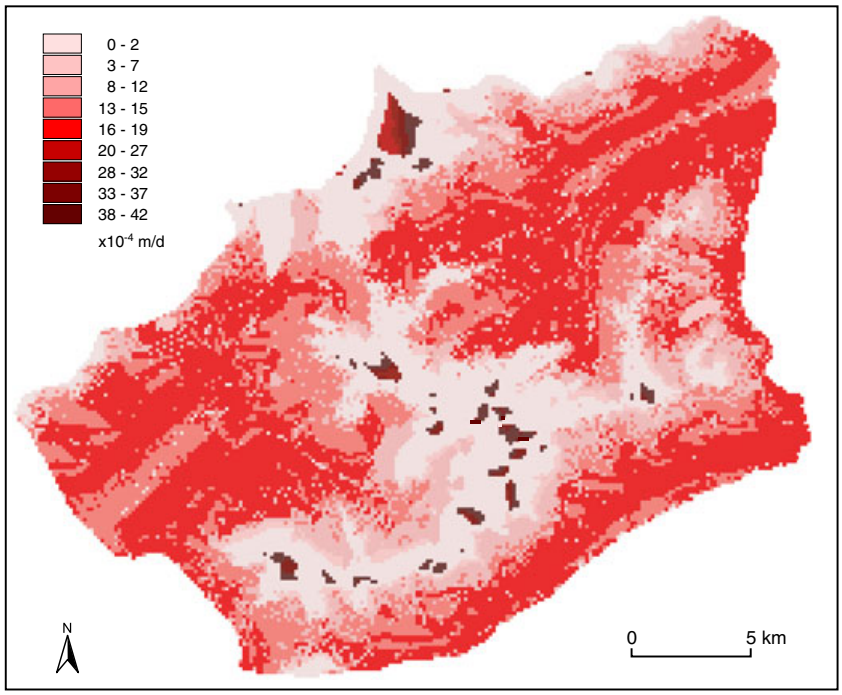

Figure 5. Map view of the distributed groundwater recharge rates applied in the groundwater flow model

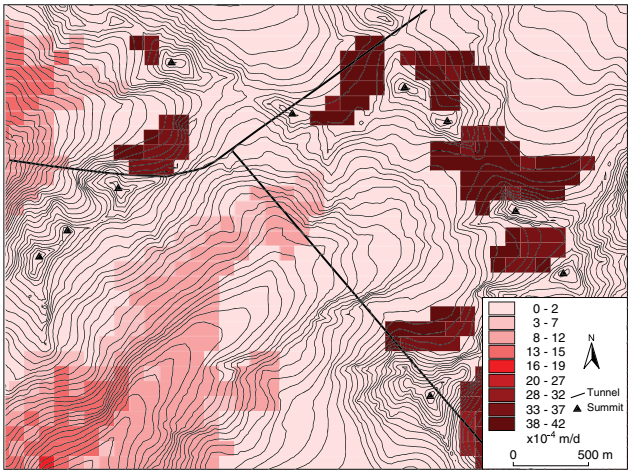

Figure 6. Enlarged map view of the distributed groundwater recharge rates in the upper Gerental-valley, applied in the groundwater flow model

conceptual discrepancy might lead to a systematic error in the spatial distribution of the recharge rates, as with regard to the overall water budget, the wrongly assigned infiltrating waters in the potential exfiltration zones would need to be attributed to other parts of the catchment to achieve a similar hydrograph simulation. For the purpose of the numerical simulations, an average recharge rate distribution was extracted from the nine-year average. The spatial average recharge rate of this distribution for the whole model domain is 12.05×10^{-4} m/d, which is in agreement with studies in similar topographic and geological settings in the Central Alps (Koella, 1993) giving a range of 2.7×10^{-4} m/d to 21.9×10^{-4} m/d with a most probable value of 10.9×10^{-4} m/d.

Flow porosities

For the calculation of isochrones in the subsequent modelling, an estimate of the flow porosity (kinematic porosity) n_f for the fractured Rotondo granite was required. This flow porosity was estimated from the transmissivity data obtained in the borehole tests and the frequencies of the fracture sets mainly associated to tunnel inflows. First, the apparent hydraulic aperture e of the flowing fractures intersected by the borehole was estimated on the basis of the cubic law:

$$e = \sqrt[3]{\frac{12T\mu}{\rho g}} \tag{3}$$

with T as the hydraulic transmissivity (m^2/s), μ, the viscosity (kg/m s), ρ, the fluid density (kg/m^3) and g, the gravitational constant (m/s^2). The results are then used to estimate a range of porosities according to the following:

$$n_f = \frac{e}{L} \tag{4}$$

where L is the measured average flowing fracture spacing (Himmelsbach *et al.*, 1998). Comparison of these results were also made to fracture porosities approximated from the empirical relation of Snow (1968):

$$n_f = 5.45\left(\frac{k_i}{L^2}\right)^{\frac{1}{3}} \tag{5}$$

with k_i as the intrinsic permeability (m^2) and L, the average flowing fracture spacing (m). As L was set to equal the spacing of the fracture sets observed to be mainly associated to tunnel inflows, and no discrimination within these sets of the spacing of specific flowing fractures was made, the flow porosities derived on the basis of L represent a potential overestimation of the actual porosity.

The so calculated values are assumed to represent the flow porosities of the more intact granite sections with moderate fracturation (blocks, n_{fB}). Calculated values for n_{fB} range from 2.4×10^{-5} to 2.9×10^{-4} and are in agreement with published values for similar rock types (Abelin *et al.*, 1991; Guimera and Carrera, 1997). For the approximation of an average flow porosity for the Rotondo granite on a larger scale, the discrete small-scale faults as well as the studied major fault zone (which in turn also consists of several discrete small-scale faults) within the granite also have to be accounted for. Flow porosities for these features (n_{fF}) could not be directly estimated, but published values for n_{fF} indicate a range from 1.3×10^{-3} (Himmelsbach *et al.*, 1998) to 7.4×10^{-3} (Frick, 1994). Based on these values, an average flow porosity for the Rotondo granite on the regional scale (n_{fRG}) was approximated by averaging the flow porosities of the faults and of the granite blocks along the approx. 1.5-km tunnel profile, weighted by the measured width of these sections along the tunnel profile following

$$n_{fRG} = \frac{\Sigma W_F \times n_{fF} + \Sigma W_B \times n_{fB}}{W_T} \tag{6}$$

where W_F (m) is the measured width of the encountered small-scale faults along the tunnel section, and W_B (m) is the width of the intermediate more intact blocks of granite. W_T (m) is the total length of the tunnel profile. Inserting the previously mentioned range of values for n_{fB} and n_{fF} yields an estimate for the average flow porosity of the Rotondo granite n_{fRG} ranging from 2.0×10^{-4} to 1.0×10^{-3}.

CONCEPTUAL MODEL

Many approaches are currently available for the simulation of flow in fractured rocks (Smith *et al.*, 1990a; NRC, 1996), each corresponding to a different conceptualization of the medium, ranging from viewing the medium as an equivalent continuum with either single or double porosity based on prescribing effective hydraulic parameters (e.g. Carrera *et al.* 1990) to associating flow only to fractures with the need for defining the geometry of the fracture network (Long *et al.*, 1982; Dverstorp and Andersson, 1989; Cacas *et al.*, 1990a, b, c). A combination of the two mentioned approaches, that is the so-called hybrid models, consists of treating minor fractures and the rock matrix as a continuum and explicitly modelling major fracture zones

(Kimmermeier *et al*., 1985; Carrera and Heredia, 1987). In addition, the channelling network concept reduces the 2D flow through the fracture planes to a 1D channel lying in the fracture plane (Neretnieks, 1983).

As this study is focused on the groundwater flow systems on the scale of the entire Rotondo massif and its interactions with the subsurface galleries, we choose a continuum approach with one discrete model fault zone to analyse the groundwater flow at this scale. Effective hydraulic conductivities are introduced into the model to characterize the hydrogeological units. A fully three-dimensional model is chosen to simulate the influence of the complex topography and the subsurface galleries on the flow systems. The effect of spatially distributed groundwater recharge rates is studied by assigning a free and movable water table. The investigated model fault zone within the Rotondo granite is represented in a discrete manner with three-dimensional elements having anisotropic hydraulic parameters. Hydraulic anisotropy of the bedrock is introduced on the basis of field observations of structural anisotropy and preferred orientations of water conducting features. The focus of the investigation and thus the modelling effort is aimed at the investigation of the groundwater flow systems within the Rotondo granite. However, as the position of the water divides is uncertain because of the anticipated effects of the tunnel galleries and the complex topography, the model domain is laterally extended to include neighbouring formations and topography. Even though this introduces additional uncertainty into the model due to badly constrained effective hydraulic parameters for these units, we consider this to be less crucial than prescribing wrong boundary conditions close to the area of interest.

NUMERICAL MODEL

The simulations of the groundwater flow in the research area were carried out with the finite element FEFLOW-code (Diersch, 1998). The mesh consists of 141 022 nodes and 259 156 elements distributed over 13 layers. Topography was extracted from the digital elevation model on a 25 × 25-m grid. The model base is at 0 m a.s.l. The total projected area of the model domain comprises approx. 262 km^2. The mesh was densified along the tunnel traces, in areas of complex topography and along the trace of the model fault zone and the rivers/streams. The top three layers of the model were kept subparallel to topography, whereas the layers below are referenced in orientation subparallel to the trace of the subsurface galleries. This vertical discretization was chosen to enable a better resolution of the free and movable water table, to assign depth dependent *k*-values and to achieve a densified discretization around the galleries. The outer boundary conditions of the domain are set impervious (no-flow conditions). The perennial streams and rivers are treated as fixed head inner boundary conditions. From the results of the hydrological model, the spatially distributed long-term mean recharge rates were extracted as upper boundary condition for the model. The Furka Tunnel and the Bedretto Tunnel are represented as line sinks with fixed elevation heads. Initial conditions for steady-state simulations are fully saturated conditions.

Modelling approach

The stable behaviour over time of the parameters measured in the subsurface (inflow rates and hydrochemical/isotopic composition of groundwater (Ofterdinger *et al*., 2004) indicates that steady-state simulations are a feasible approach to calibrate effective *k*-values. Calibration efforts are carried out in a trial and error procedure and are focused on the Rotondo granite and the immediate adjacent formations in order to reach a correlation to the observed inflow rates at the Bedretto Tunnel and the Furka Tunnel.

In a first phase, *k*-values for the Rotondo granite and/or the fault zone within the granite are adapted to achieve the observed discharge rates to the Bedretto Tunnel. Secondly, to match the measured inflow to the Furka Tunnel, especially along the section through the northern margin of the granite body, additionally, *k*-values for the northern gneisses (O, PN) are adjusted to achieve a model calibration. The recorded head data from the research borehole and the position of the spring line on the terrain surface serve as additional criteria to assess the plausibility of the modelling results. During the modelling process, three base case scenarios are evaluated in which we address the impact of the model fault zone and the subsurface galleries on the groundwater flow system.

In scenario 1, a calibration is sought for a continuum numerical model without including the higher conductive fault zone.

In scenario 2, an isotropic higher conductive fault zone (FZ) is incorporated into the model with a *k*-value contrast to the surrounding granite bedrock (G) of 1:10 ($k_{FZ} = 10 \times k_{1G}$).

In scenario 3, anisotropy is introduced within the fault zone of scenario 2. The anisotropy ratio is set to $k_{1FZ} = k_{3FZ} = 10 \times k_{2FZ}$, with k_2 representing the fault-normal flow direction.

The influence of the subsurface galleries on the groundwater flow field within the Rotondo Granite is investigated for all model scenarios by removing the fixed head inner boundary conditions associated with the galleries.

In a sensitivity study following the model calibration of the individual scenarios, the influence of varying recharge conditions is addressed. Model simulations with a series of spatially uniform recharge rates are compared with the model results with spatially distributed groundwater recharge rates. As values for the uniform recharge rates, the spatial average recharge rate for the whole model domain (12.05×10^{-4} m/d or 19% of mean annual precipitation), the spatial average recharge rate for the upper Gerental catchment (region above the Bedretto Tunnel, 5.75×10^{-4} m/d or 7% of mean annual precipitation) as well as a minimal value of 2.74×10^{-4} (approx. 3% of mean annual precipitation) were chosen. These values lie in the range of published recharge rates for granitic terrain, ranging from 2–21% of mean annual precipitation (Lerner *et al*., 1990; Koella, 1993). Table V summarizes the approach to the individual model scenarios and model variants.

Table V. Summary of key characteristics of individual model scenarios and model variants

Model	Description
Scenario[†]	
1	Higher conductive fault zone not included
2	Isotropic higher conductive fault zone included ($k_{FZ} = 10 \times k_{1G}$)
3	Anisotropic higher conductive fault zone included ($k_{1FZ} = k_{3FZ} = 10 \times k_{2FZ}$)
Variant[‡]	
1	Spatially uniform recharge rate applied (5.75×10^{-4} m/d)
2	Spatially uniform recharge rate applied (12.05×10^{-4} m/d)
3	Spatially uniform recharge rate applied (2.74×10^{-4} m/d)

FZ, fault zone; *G*, granite; k_{2FZ}, fault-normal flow direction.
[†] Spatially distributed recharge rates are applied to individual model scenarios (refer to Section 'Groundwater Recharge Rates').
[‡] Model variants are based on calibrated model scenario 2.

For all model variants, particle tracking is carried out to delineate the respective recharge areas to the Bedretto Tunnel. Particle backtracking is started along the mesh nodes representing the Bedretto Tunnel as well as along the projected nodes on the 5 m overlying and underlying mesh slice. Additionally, forward tracking was initiated from the top slice of the model to cross-check the delineated recharge areas. Finally, isochrones were calculated along the pathlines, initiated at the tunnel nodes, to approximate the advective travel times across delineated recharge areas to the Bedretto Tunnel.

Model calibration

Scenario 1. To reach the calibration target of groundwater inflow to the Bedretto Tunnel, the *k*-value of the Rotondo granite had to be adjusted to $k_1 = 1.2 \times 10^{-8}$ m/s (Table VI). This value may range from 1.15×10^{-8} m/s to 1.25×10^{-8} m/s to still meet the calibration target. To achieve a calibration for the granite section along the Furka Tunnel, the *k*-value of the northern adjacent gneiss-unit (O) was additionally reduced by a factor of 0.4, and the *k*-value of the neighbouring PN-unit had to be reduced by one order of magnitude from the initial value to match the flow rates at the Oberwald-Portal of the Furka Tunnel. To further match the inflow along the section of the Furka Tunnel, which drains towards the Realp-Portal (Figure 4), the *k*-value for the Cacciola-granite was increased to $k_1 = 8.0 \times 10^{-8}$ m/s. This is regarded as plausible because major inflows along the Cacciola section of the Furka Tunnel are reported (Keller and Schneider, 1982). The calibrated *k*-value for the Rotondo granite is in good agreement with the first approximations following the analytical solution (Table III). Simulated heads in the monitoring intervals are underestimated by the flux-calibrated model (Table VI). Furthermore, Figure 7 shows that this model scenario without the fault zone is not able to reproduce the cumulative inflow along the Bedretto Tunnel.

Scenario 2. With the fixed *k*-value contrast between the granite bedrock and the fault zone of 1:10, a calibration to the inflow rate along the fault zone section of the Bedretto Tunnel as well as to the inflow rate along the remaining bedrock section was reached with *k*-values of 6.0×10^{-9} m/s and 6.0×10^{-8} m/s for k_1 of the granite and the isotropic fault zone, respectively. These values are again in good agreement with the analytical approximations. Variation of the respective *k*-value for the granite bedrock and the fault zone within one order of magnitude yield inflow rates to the Bedretto Tunnel beyond the calibration target. An increase of the absolute *k*-values of the granite and the fault zone to $8.0 \times 10^{-9}/8.0 \times 10^{-8}$ m/s leads for example to inflow rates to the Bedretto Tunnel and the fault zone section of 19.3 and 10.3 l/s, respectively. A decrease of *k*-values to $5.0 \times 10^{-9}/5.0 \times 10^{-8}$ m/s yields discharge rates of 12.3 and 6.7 l/s for total inflow to the Bedretto Tunnel and the fault zone section. To achieve a match to the inflow along the Rotondo granite section of the Furka Tunnel, the *k*-values of the neighbouring gneiss (O) had to be increased compared with scenario 1 by a factor of 0.6 from the initial value. The cumulative inflow along the Bedretto Tunnel for the calibrated model approximates well the measured inflow profile (Figure 7). However, similar to scenario 1, the heads in the monitoring intervals are underestimated (Table VI).

Table VI. Calibration targets for inflow rates along specific tunnel sections and hydraulic heads in monitoring intervals with calibrated values for the individual model scenarios

	Calibration target	Scenario 1	Scenario 2	Scenario 3
		Tunnel inflow rates		
Tunnel section	[l/s]	[l/s]	[l/s]	[l/s]
Bedretto	14.9 ± 0.5	14.8	15.0	15.2
Fault Zone	7.5 ± 0.5	(1.9)	7.7	7.8
Furka (RG)	25.8 ± 5.6	25.2	21.8	21.8
Oberwald	94.4 ± 5.9	95.0	91.6	89.7
Realp[†]	75.8 ± 5.9	70.9	72.9	73.2
		Hydraulic heads		
Monitoring Interval	[m]	[m]	[m]	[m]
Interval 1	1988	1819	1851	1850
Interval 2	1894	1756	1782	1781

[†] Only four measurements 1998–March 1999.

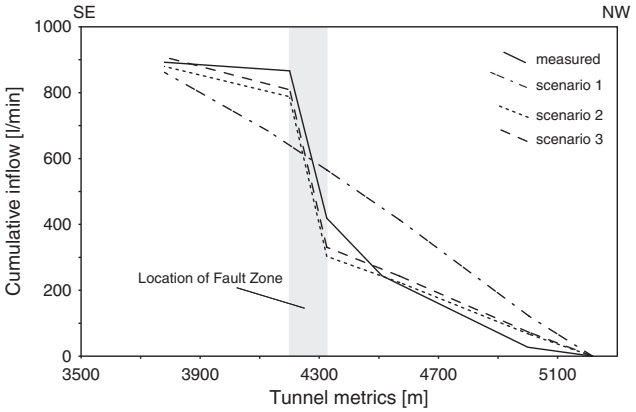

Figure 7. Plot of measured cumulative groundwater inflow to the Bedretto Tunnel along the tunnel profile versus simulation results for the individual model scenarios. The whole tunnel section is situated within the Rotondo granite. For tunnel metrics, refer to Figure 4

Scenario 3. The introduction of anisotropy within the fault zone (base case $k_1 = 10k_2$ with k_2 fault-normal orientated) into the calibrated model of scenario 2 causes only a slight decrease in fluxes to the Bedretto Tunnel (-0.8 l/s for the total tunnel from which -0.6 l/s along the fault zone section). *K*-values were adjusted to 6.5×10^{-9} and 6.0×10^{-8}m/s for the Rotondo granite and the fault zone respectively to reach the calibration targets. A small additional increase of the *k*-values to $7.0 \times 10^{-9}/7.0 \times 10^{-8}$ m/s leads to tunnel inflow beyond the calibration target of 16.3 and 8.4 l/s for the Bedretto Tunnel and the fault zone section, respectively. The cumulative inflow along the Bedretto Tunnel resembles the simulation results of scenario 2. Similar to the previous scenarios, the model fails to reproduce the local head measurements in the monitoring intervals (Table VI).

Model results

In all model scenarios, a considerable decline of the water table below topography is simulated along the mountain crests within the Rotondo area, especially along the trace of the subsurface galleries. For scenario 1, simulated position of the water table range from ≤200 m below the ridges above the Furka Tunnel in the orthogneiss to up to 600 m below the crests of the Saashörner ridge in the Rotondo granite (Figure 8). In the east of the model domain, deep groundwater tables can be observed in the Winterhorn and Siroerbenhorn area. In the western part of the domain, the groundwater table lies at 100–300 m below the ridges of the Mettligrat and Mittaghorn. In the Blauberg area to the north of the domain, depth to the groundwater table reaches 200 m.

In scenario 2, the decline of the water table below topography is less pronounced. Depth to the groundwater table reaches up to 300 m below the Saashörner and up to 250 m above the Furka Tunnel in the Rotälligrat area (Figure 9). No additional decline of the water table due to the introduction of the higher conductive fault zone is observed. The position of the groundwater table for scenario 3 resembles closely the simulation results of scenario 2.

Even though the water table position in the core of the massifs differ significantly between model scenarios the observed altitude of the spring discharges in the study area (Figure 2) is reproduced by all model scenarios within an accuracy of 20–100 m. The inaccuracy leads thereby to an overestimation of the spring line altitude.

For all three model scenarios, the particle tracking delineates recharge areas to the Bedretto Tunnel lying mainly along the crests of the high mountain ridges. The upper glacier regions present here essentially the main

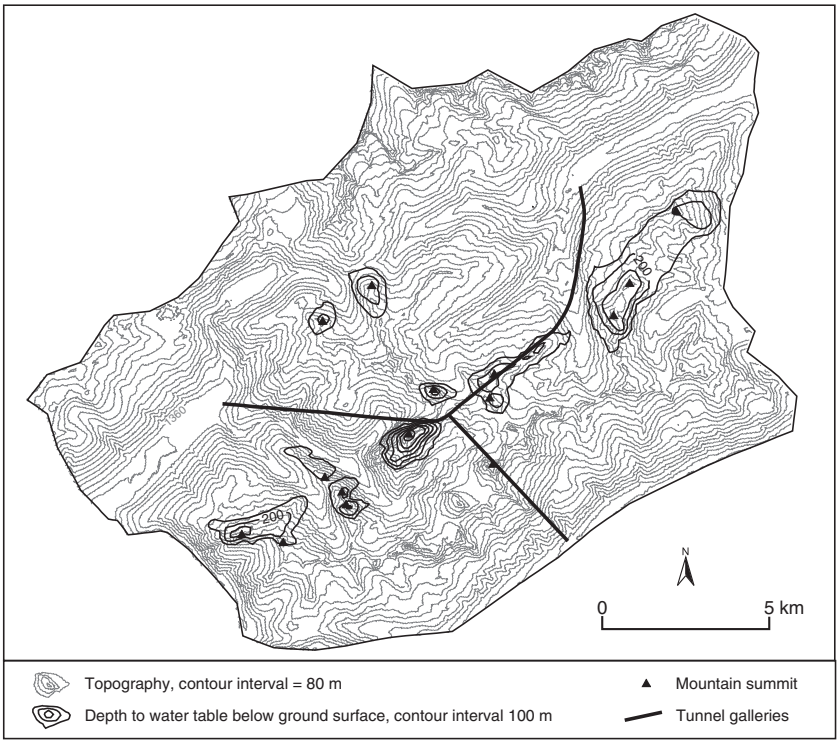

Figure 8. Depth to the groundwater table below ground surface for model scenario 1. Also indicated are several mountain summits for better orientation

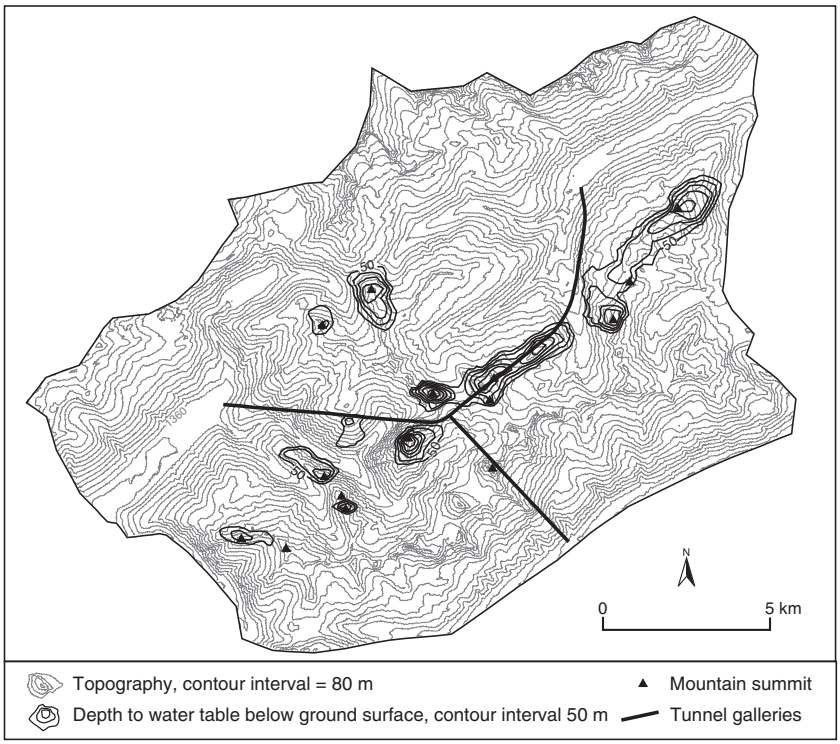

Figure 9. Depth to the groundwater table below ground surface for model scenario 2. Also indicated are several mountain summits for better orientation

recharge source to the gallery (Figure 10). An additional recharge area is situated along the mid-altitude southern slope of the Sasshörner, along a smaller valley inward trending ridge. Here, moderate recharge rates are predicted by the hydrological model (Figure 6). In all three scenarios, the northern end of the Bedretto Tunnel is recharged from the glaciated areas of the Leckihorn and Saashörner area as well as from the previously mentioned

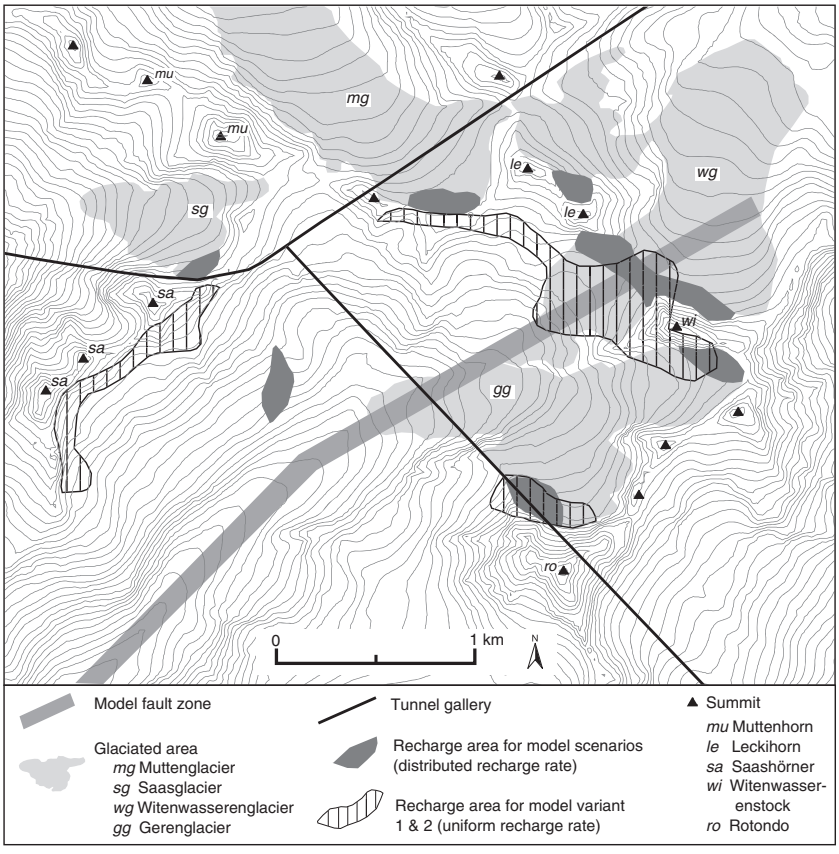

Figure 10. Enlarged plan view of the upper Gerental-valley with the position of the recharge areas to the Bedretto Tunnel for the model scenarios and model variants 1 and 2

recharge area along the Saashörner slope. The fault zone section along the Bedretto Tunnel is recharged from the glaciated area at the Witenwasserenpass area (between Leckihorn and Witenwasserenstock) in the east and from the glaciated regions on the north-facing slope of the Rotondo.

The introduction of the higher conductive fault zone in scenarios 2 and 3 into the model leads to an enlargement of the recharge area, in particular in the upper regions of the Witenwasserenglacier. Flow entering the fault zone is aligned with the fault zone orientation and directed to its intersection with the gallery. For the southern end of the accessible part of the Bedretto Tunnel, the particle tracking indicate the upper region of the Gerenglacier as recharge area.

To assess the influence of the subsurface galleries on the groundwater flow system in the Rotondo area, all calibrated model scenarios were additionally simulated without the fixed head boundary condition along the tunnel profile. Simulated heads without the tunnel condition show significantly less decline of the water table below ground surface. For scenario 1, this head difference between simulations with and without tunnel amounts to 350 m in the Saashörner area, 50–150 m along the Rotälligrat and approx. 50 m in the Siroerbenhorn area (Figure 11). For scenarios 2 and 3, these differences range from up to 150 m along the Saashörner to 50–100 m and 50–150 m along the Rotälligrat and Siroerbenhorn, respectively. With regard to the particle tracking, all model scenarios show that without the tunnel gallery, only the eastern part of the previously described recharge areas, that is, the area of the Leckihorn to Gerenglacier, is drained towards the tunnel position. This influence of the gallery on the natural flow field is also illustrated in Figure 12, where the influence of the Bedretto Tunnel is shown to cause a strong modification of head gradients.

Advective travel times from the individual recharge areas were estimated from the calculated isochrones along the pathlines, initiated at the tunnel nodes, and are given in Table VII. The range of values for the applied flow porosities n_{fRG} yields a wide range of 1 to 14 years for flow from individual recharge areas to the gallery (Table VII). In a relative comparison amongst the estimated travel times, the rapid flow path via the fault zone is apparent (Figures 13 and 14).

Sensitivity study

The particle tracking for the individual model scenarios show that the prescribed distributed recharge rates strongly influence the position of the tunnel recharge areas and type of recharge source, that is recharge from glaciers or mountain slopes. Recharge is hereby dominated by the high recharge rates in the upper regions of the glaciers. To assess the impact of a change in the recharge conditions, three model variants with different uniformly distributed recharge rates are considered and applied exemplarily to model scenario 2. As described before, recharge rates are thereby varied within a plausible range of potential recharge rates. Note that simulations with uniform recharge rates are referred to in the following as '*model variant*' opposed to the calibrated simulations (*model scenarios*).

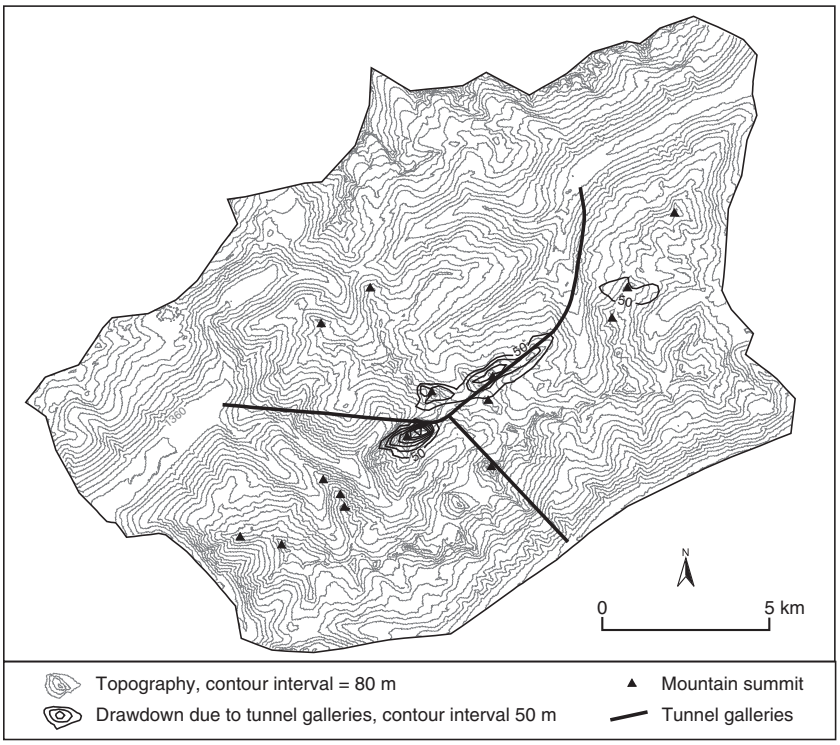

Figure 11. Plan view of the model domain with isolines of drawdown due to tunnel galleries for model scenario 1. Also indicated are several mountain summits for better orientation

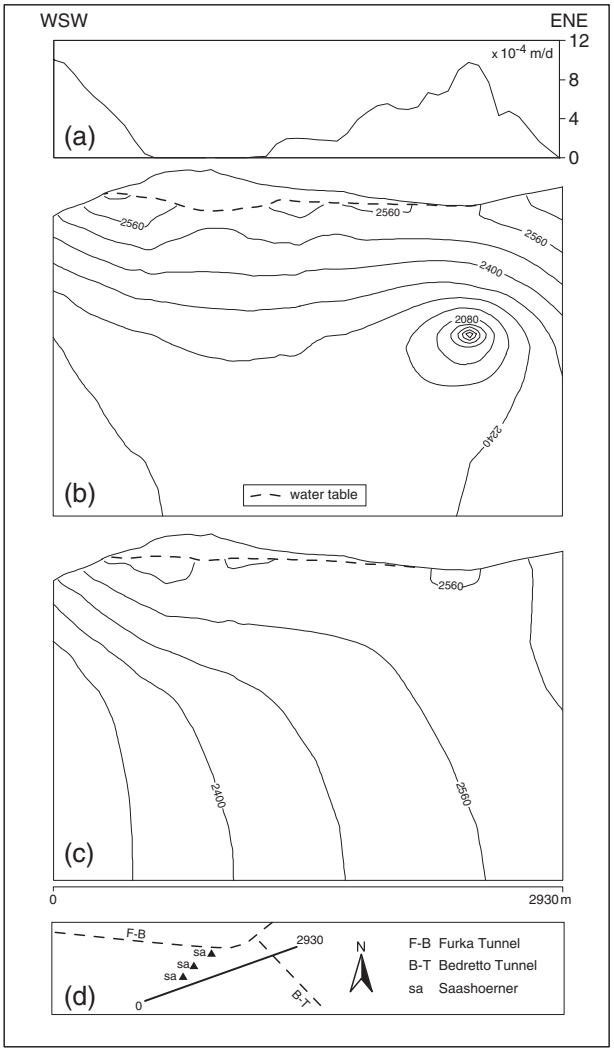

Figure 12. Two-dimensional section of hydraulic potentials for model scenario 3. (a) Groundwater recharge rates extracted along the profile section and interpolated on 50-m intervals along the section; (b) 2D section of hydraulic potentials and position of groundwater table for model scenario 3 simulated with the tunnels; (c) corresponding section for model scenario 3 simulated without tunnels; and (d) schematic plan view of the location of the profile section in the upper Gerental-valley (refer to Figure 2). The vertical exaggeration of(b) and (c) is 0.7

Table VII. Approximated advective travel times across recharge areas for model scenarios, deduced from calculated isochrones along path lines initiated at the Bedretto Tunnel nodes

Recharge area	Travel times [years]	
	$n_{fRG} = 2.0 \times 10^{-4}$	$n_{fRG} = 1.0 \times 10^{-3}$
Leckihorn	2–3	8–10
Witenwasserenstock	2–3.5	10–14
Rotondo	2–2.5	10–12
Saashoerner	2–2.5	9–10
Witenwasserenpass (*Through fault zone*)	1–1.5	3–5

First, we consider a uniform recharge rate of 5.75×10^{-4} m/d, a value extracted from the distributed recharge rates as mean recharge rate in the upper Gerental

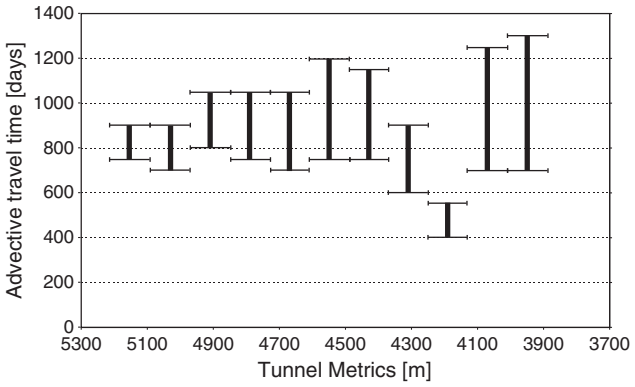

Figure 13. Range of advective travel times to the Bedretto Tunnel for 120 m intervals along the tunnel axis. Travel times are deduced from calculated isochrones along pathlines initiated at the Bedretto Tunnel nodes ($n_{fRG} = 2.0 \times 10^{-4}$)

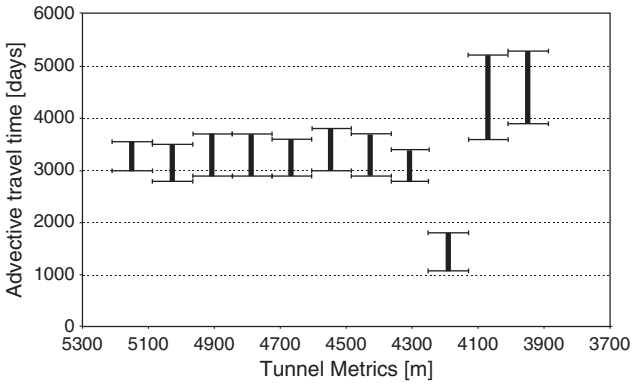

Figure 14. Range of advective travel times to the Bedretto Tunnel for 120 m intervals along the tunnel axis. Travel times are deduced from calculated isochrones along pathlines initiated at the Bedretto Tunnel nodes ($n_{fRG} = 1.0 \times 10^{-3}$)

catchment above the Bedretto Tunnel (>2000 m a.s.l., *variant 1*). We observe that the position of the water table is significantly modified in comparison with model simulation with spatially distributed recharge rates. Figure 15 shows, in comparison with Figure 9, that the position of the water table is significantly modified. No decline of the water table is observed in the Saashörner area, whereas an additional decline of the water table is located in the Witenwasserenstock and Rotondo area. An additional decline of the water table can furthermore be observed along the ridges in the east and west of the domain as well as in the Blauberg area to the north. This illustrates the strong effect of the spatially distributed recharge rates on the position of the groundwater table especially in the Saashörner area. Groundwater fluxes to the Bedretto Tunnel are only changed by 2–3 % and fluxes to the Rotondo granite section of the Furka Tunnel by 7% (Table VIII). Changes in the simulated heads in the monitoring intervals are only minor (Table VIII). The locations of the recharge areas to the Bedretto Tunnel are strongly affected by the change in recharge conditions, especially to the west of the gallery (Figure 10). Here, the recharge area is now situated along the entire ridge of the Saashörner. No more drainage from the Saasglaciers

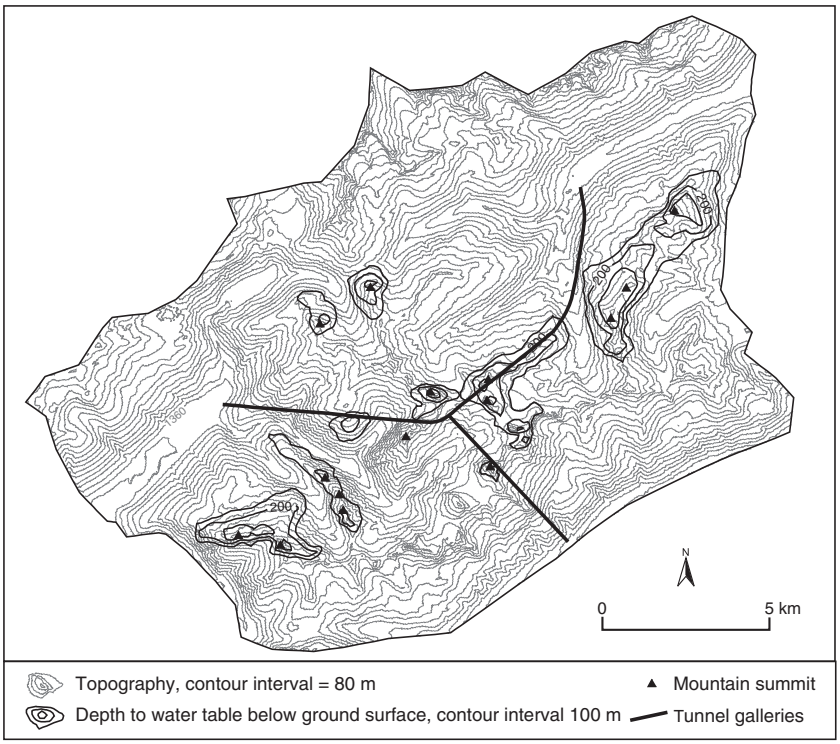

Figure 15. Depth to the groundwater table below ground surface for model variant 1 with uniform groundwater recharge of 5.75×10^{-4} m/d. Also indicated are several mountain summits for better orientation

Table VIII. Simulated groundwater inflows to the tunnel galleries and simulated heads in the monitoring intervals for model variants with uniform groundwater recharge rates

	Variant 1	Variant 2	Variant 3
	Tunnel inflow rate		
Tunnel section	[l/s]	[l/s]	[l/s]
Bedretto	14.7	15.1	13.6
Fault zone	7.5	7.6	7.0
Furka (RG)	19.1	18.3	14.8
Oberwald	86.4	86.7	65.0
Realp	69.2	72.6	64.5
	Hydraulic heads		
Monitoring interval	[m]	[m]	[m]
Interval 1	1847.0	1854.6	1774.5
Interval 2	1779.1	1784.8	1719.1

Variant 1: 5.75×10^{-4} m/d.
Variant 2: 12.05×10^{-4} m/d.
Variant 3: 2.74×10^{-4} m/d.

and Muttenglaciers occurs. The recharge area to the east of the Bedretto Tunnel is shifted downslope in the Leckihorn area towards the west. Recharge areas to the fault zone are still situated along the glaciated area of the Witenwasserenpass, with an increased area towards lower elevations, and along the southern Rotondo slope.

With a higher uniform recharge rate of 12.05×10^{-4} m/d (*variant* 2) extracted from the distributed recharge rates as mean recharge rate for the entire model domain, generally less decline of the water table below the ground surface can be observed when compared with the results from model scenario 2. No decline of the water table below the Saashörner ridge can be observed. Also, the depth to the groundwater table in the Rotälligratt area is decreased. In the eastern and western parts of the model domain (Winterhorn and Mettligrat area), changes are only minor. Changes in the groundwater flux to the galleries are minor with 1–2% in the Bedretto Tunnel and 1–5% in the Furka Tunnel (Table VIII). Changes in simulated heads for the monitoring intervals are also only minor. The delineated recharge areas to the Bedretto Tunnel are similar to those deduced for the model variant 1.

In a third variant, the uniform groundwater recharge rates are reduced to 2.74×10^{-4} m/d, a value at the lower end of plausible recharge rates. This low uniform recharge rate has a dramatic effect on the position of the groundwater table elevation in the model domain (Figure 16). Large areas, not only restricted to the crest regions of the mountain ridges, show considerable decline of the water table below the ground surface. The water table is in fact declined closely to the valley bottom in the upper Gerental catchment with considerable decline also along the trace of the Bedretto Tunnel across the upper Gerental valley. The depth to the groundwater table amounts to 400–600 m in the Winterhorn, Saashörner and Siroerbenhorn area. In the Leckihorn and Witenwasserenstock area, depths to the water table also reach 400–600 m. The decline of the water table extends below the Muttenglacier and Witenwasserenglacier and reaches 100–200 m above the Bedretto Tunnel. The effect of this change in recharge rate is also manifested in a clear change in groundwater fluxes to the Bedretto and Furka Tunnel with changes of 9–10% and 12–30%, respectively

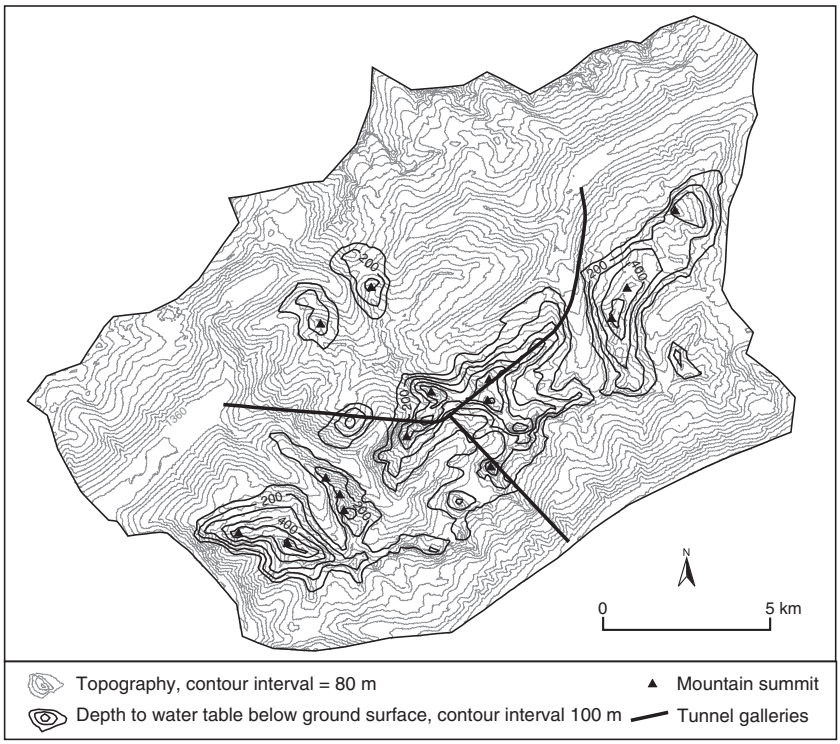

Figure 16. Depth to the groundwater table below ground surface for model variant 3 with uniform groundwater recharge of 2.74×10^{-4} m/d. Also indicated are several mountain summits for better orientation

(Table VIII). Also, the simulated heads in the monitoring intervals show a significant decrease (Table VIII). The recharge areas are drastically modified. To the west, a large area along the Saashörner slope is recharging to the Bedretto Tunnel. Likewise to the east, the slopes of the Leckihorn are recharging to the gallery. Essentially a broad area from directly above the tunnel trace and expanding to the west to the Sasshörner and to the east to the Leckihorn area are drained to the Bedretto Tunnel. The recharge area to the fault zone is still largely situated along the Witenwasseren- and Gerenglacier.

Discussion of model results

The modelling of the previously mentioned scenarios in steady-state simulations show that the calibrated *k*-values are generally in good agreement with the analytical a priori estimates. With regard to the hydraulic conductivities of the individual geological units, the modelling process showed that the fluxes to the Bedretto Tunnel are mainly governed by the prescribed *k*-value within the Rotondo granite, whereas the inflow along the granite section to the Furka Tunnel are additionally sensitive to the *k*-values of the orthogneisses. Changes in hydraulic conductivity of the Rotondo granite in the range of less than one order of magnitude hereby cause observable differences in the elevation of the groundwater table, especially in the Saashörner area.

The model simulations yield regional and local groundwater flow systems within the Rotondo area whereby the regional scale groundwater flow is mainly directed towards the Rhône-valley in the east and the Ticino-valley at the southeastern border of the model domain. Unsaturated zones below the ridges and crests of up to several hundred metres are observed (Figures 8 and 9). The depths to the groundwater table below the Saashörner and along the eastward section of the Furka Tunnel are enhanced by the presence of the subsurface galleries (Figure 11). Simulated pronounced decline of the water table in the Saashörner area are confirmed by the findings of a nuclear magnetic resonance survey along the southern slopes of this ridge, indicating a depth to the water table of >90 m (Legchenko *et al*., 1998). The presence of the subsurface galleries in the Rotondo area causes strong modifications of the natural head gradients, leading locally to a reversal of natural groundwater flow directions (Figure 12).

The introduction of a higher conductive fault zone within the base case scenario leads to a modification of the head distribution in the model domain, as the hydraulic conductivity of the surrounding bedrock was adapted to match the measured flow rates to the galleries. The ratio of anisotropy within the fault zone is of only little significance in the simulated scenarios. This is most probably linked to the overall orientation of the fault zone sub-parallel to the main flow field and the regional anisotropy of hydraulic conductivity within the adjacent bedrock. Thus, a potential barrier effect in fault-normal direction due to a high ratio of anisotropy within the fault zone would not significantly hinder the natural fault-parallel oriented flow field.

Heads in the monitoring intervals of the research borehole, characterizing the head distribution in a moderately fractured part of the granite body, are underestimated in

all flux-calibrated model scenarios. Modifications of the *k*-value contrast between the granite bedrock and the fault zone from the originally set contrast of 1:10 does not provide a better match of both inflow and the local head data. For example, a decrease of the *k*-value of the Rotondo granite in scenario 2 to a value of 1.0×10^{-9} m/s, while maintaining the hydraulic conductivity of the fault zone at 6.0×10^{-8} m/s results only in an increase of simulated heads in the monitoring intervals of 21 m (interval 1) and 17 m (interval 2), respectively. At the same time, simulated groundwater inflow to the Bedretto Tunnel is already reduced by as much as 5.4 l/s. This amount cannot be compensated for by a potential increase of the fault zone *k*-value without exceeding the measured calibration target for the inflow along the fault zone section. This model behaviour indicates that the presented equivalent continuum approach with only a single discrete higher conductive fault zone is not able to simultaneously reproduce the measured flow to the gallery and the local head data from the research borehole correctly. For a match of both flux and head data, further discrete higher conductive features would need to be included into the model. This would then essentially lead to lower *k*-values for the granite bedrock in the calibration process and thus to an increase of simulated heads at the borehole site.

Generally, the model simulations reproduce well the position of spring discharge in the upper Gerental valley. As these are situated only a few decametres to hundred metres above the valley floor along the steep slopes, the influence of the conceptual discrepancy between the modelled exfiltration zones and the recharge areas predicted along the valley floor by the hydrological model as stated earlier is thought to be less significant. The area concerned is rather small compared with the scale of the massif.

Applying the groundwater recharge rate distribution from the hydrological model to the individual model scenarios yields similar catchment areas to the Bedretto Tunnel. In the framework of this prescribed recharge distribution, the catchment areas are mainly associated to the glaciated areas with high recharge rates. The inflows to the fault zone section along the Bedretto-tunnel are in all model scenarios consistently recharged by the glaciated areas of the Witenwasserglacier and Gerenglacier.

The distribution of delineated recharge areas is shown to be strongly dependent on the spatial distribution of the recharge rates within the model domain. In the prescribed distributed recharge rates, the most striking feature is the strong contrast at high altitudes between the steep bare rock slopes with little or essentially zero recharge and the upper regions of the glaciers, where high recharge rates are predicted (Figure 5 and 6). These strongly localized high recharge rates dominate the delineated recharge areas.

The effect of the spatial discretization of the recharge rates is apparent when compared with the results from the simulations with an equivalent uniform mean recharge rate. The recharge areas to the Bedretto Tunnel are now more broadly aligned along the mountain ridges, and, especially to the west, a wider area along the Saashörner ridge is recharging to the Bedretto Tunnel (Figure 10). With a uniform recharge rate, the fault zone section in the tunnel is consistently recharged from the area of the Witenwasserenglacier and Gerenglacier. Additionally, the lower slopes of the Gerenglacier are recharged along the fault zone to the Bedretto Tunnel. The groundwater fluxes to the Bedretto Tunnel are only affected to a minor degree, when an average uniform recharge rate is extracted from the spatially distributed recharge rates of the upper Gerental (*variant* 1) or the whole model domain (*variant* 2), respectively. However, when the absolute value of the uniform recharge rate is lowered to a minimum plausible value (*variant* 3), dramatic changes in terms of recharge area, water table position and tunnel inflows are observed (Figure 16, Table VIII). The latter are decreased clearly below measured inflow rates to the galleries. Forster and Smith (1988a) investigate the nonlinear fashion in which the water table elevations respond to changes in groundwater recharge rate. The response of the water table elevation in the Rotondo granite (below the Saashörner) appears to be illustrating this nonlinear behaviour.

Comparing the position of the water table for the individual model scenarios and variants (Figures 8, 9, 15 and 16), the magnitude of variations in water table elevation below the Saashörner is striking. One explanation for this sensitive behaviour lies in the specific topography, that is the high relief of this mountain. The Saashörner are bound to three sides by deep valleys, especially to the north and west with steep slopes ranging from 1800 to 2900 m.a.sl. To the east, the subsurface galleries impose an additional low fixed head boundary. The surrounding crests including the Leckihorn and Rotälligrat are aligned along elongated mountain ridges, show less steep relief and bounding valleys are generally at an altitude >2000–2100 m a.s.l. Model simulations of Forster and Smith (1988b) have also shown that high-relief terrain amplifies the impact of factors such as permeability and recharge rate on groundwater flow systems within mountain massifs.

As a consequence of the sensitivity study, the eastern recharge areas can be regarded as robust, because they are delineated by all model variants as recharge areas, independent of the recharge conditions. The position of the recharge areas to the west of the Bedretto Tunnel are more clearly subject to the spatial discretization of the recharge rates, and some ambiguity remains on their position. In the following, we will discuss how the environmental isotope data can supplement these interpretations.

COMPARISON WITH RESULTS FROM ENVIRONMENTAL ISOTOPE STUDY

In a previous study of the isotopic and hydrochemical composition of the encountered groundwater along the Bedretto Tunnel (Ofterdinger *et al.*, 2004), measured

δ^{18}O values indicate an altitude effect with higher recharge altitudes towards the northern end of the Bedretto Tunnel (Figure 17). Estimated mean recharge altitudes lie in the range of 2600–2800 m a.s.l.

The numerical simulations with distributed recharge rates yield recharge areas to the northern end of the Bedretto Tunnel mainly associated with the Saasglacier and Muttenglacier as well as the Leckihorn area at elevations of 2800–2900 m a.s.l. Proceeding to the south along the Bedretto Tunnel, an additional recharge area along the Saashörner slope at elevations of 2500–2600 m a.s.l. is drained towards the Bedretto Tunnel. Along the fault zone section of the gallery, depleted δ^{18}O values diverging from the above trend are observed. A recharge altitude of approx. 2740 m a.s.l. is approximated from the isotope data. The delineated recharge area for the fault zone section from the model simulations with distributed recharge rates is situated at the glaciated Witenwasserenpass area at an elevation of approx. 2800 m a.s.l. Additionally, an area along the northern slope of the Rotondo at an elevation of 2800–2900 m a.s.l. is delineated as recharge area to the fault zone section. For the southern end, δ^{18}O values similar to the most northern end of the gallery are observed. The model simulations delineate a recharge area along the upper slopes of the Gerenglacier as recharge source to this tunnel section. A decreasing recharge altitude along the northern end of the tunnel is also reproduced in the model variants with uniform recharge rates. To the west of the Bedretto Tunnel a recharge area along the Saashörner is delineated with altitudes between 2800 and 2700 m a.s.l. and to the east of the gallery between 2900 and 2700 m a.s.l. as sampling locations in the tunnel advance southwards. The fault zone section is recharged from the Witenwasserenglacier and Gerenglacier at elevations ranging from 2700–2800 m a.s.l. to the east and 2800–2900 m a.s.l. along the Rotondo slope. Even though the range of values deduced from both recharge distributions show an agreement, it has to be stressed that the specific position and thus altitude of the recharge areas is subject to the prescribed orientation of k_1 within the Rotondo granite, which was constrained by field observations and measurements.

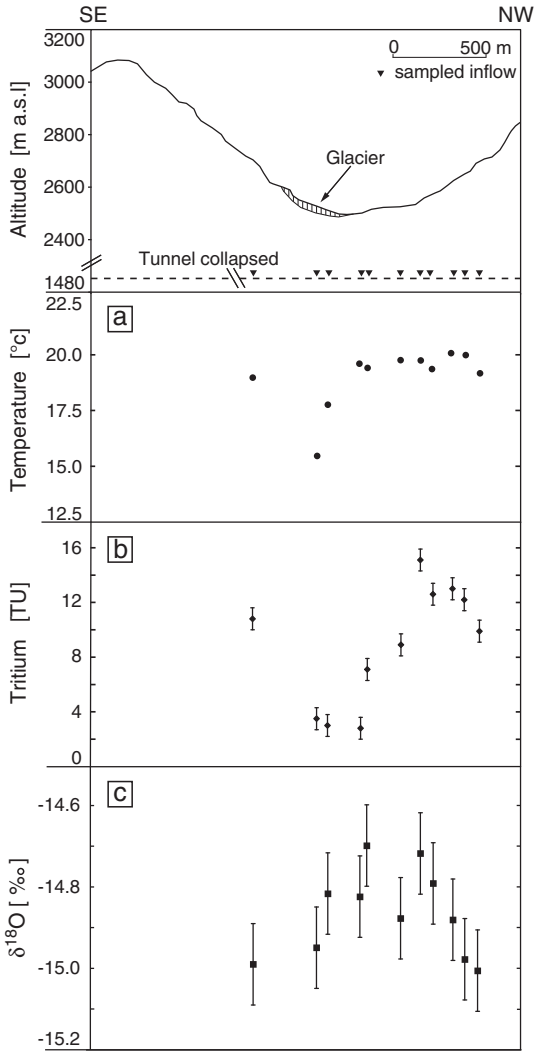

Figure 17. Cross section along the profile of the Bedretto Tunnel with location of sampled inflows; (a) mean temperature, (b) mean tritium concentration and (c) mean δ^{18}O value of sampled groundwater. The analytical error is indicated

Estimated mean residence times from lumped-parameter modelling of the δ^{18}O signature in groundwater samples taken along the fault zone section are 1–1.5 years. In the numerical simulations, the advective travel times deduced from the calculated isochrones for pathlines to the fault section of the gallery are in a similar order of magnitude, however showing a wider range from 1–5 years depending on the applied flow porosity value. Travel times to the fault zone section of the Bedretto Tunnel were furthermore estimated on the basis of tritium data in groundwater samples and recharge components (Ofterdinger, 2001; Ofterdinger *et al.*, 2004) using the decay equation (Clark and Fritz, 1997)

$$\alpha_t{}^3\mathrm{H} = \alpha_0{}^3He^{-\lambda t} \tag{7}$$

with $\alpha_0{}^3$H initial tritium concentration in groundwater recharge, $\alpha_t{}^3$H residual tritium concentration in groundwater sample (both in TU) and λ decay term $\lambda = \ln 2/t_{1/2}$ ($t_{1/2}$ = 12:43 years, half-life of tritium). These simplified calculations underline that for these range of travel times, summer precipitation is only a minor component in groundwater recharge to the fault zone section of the Bedretto Tunnel.

The tritium data measured along the Bedretto Tunnel show, that the groundwater encountered along the fault zone section is recharged from glacial melt water as a combination of melt water from accumulated low tritium winter precipitation and glacial ice melt. The contribution of sub-modern glacial ice melt thus leads to the observed low tritium values in the inflows (Ofterdinger *et al.*, 2004). All model scenarios and variants reproduce the observations of glacial recharge.

To the northern end of the Bedretto Tunnel, measured tritium values indicate recharge from recent winter precipitation (Figure 17). The model scenarios with distributed

recharge rates delineate the Saasglacier and Muttenglacier as an important recharge source to this tunnel section, whereas the model variants with uniform recharge delineate the slopes of the Saashörner as recharge area. If the Saasglacier and Muttenglacier were to contribute dominantly to the groundwater recharge to this tunnel section, the difference between the measured tritium values in this section to the observed low tritium values along the fault zone section would need to be explained by a different isotopic composition of the melt water from theses glaciers, as both tunnel sections would then be recharged essentially by the same type of recharge source. Groundwater recharge from recent accumulated winter precipitation on the slopes of the Saashörner could however explain well the measured tritium values in the northern tunnel section. The tritium data observed along the northern section of the Bedretto Tunnel is thus not in agreement with the recharge sources delineated from the simulations with the distributed recharge rates. These predict the upper regions of the glaciers as dominant recharge areas to the tunnel with high recharge rates. The dominance of these recharge areas results from the bi-modal groundwater recharge concept for the glaciated areas applied in the hydrological model. In this concept, melt water from above the equilibrium line of the glaciers preferentially contributes to the slow runoff storage and thus to groundwater recharge, whereas melt water from below the equilibrium line is attributed to the fast runoff storage. This model has been previously applied for hydrological studies in the Rhône-area (Badoux, 1999) and builds on the idea that melt water from above the equilibrium line percolates through the glacial body and crevasses towards the distributed subglacial drainage system. Here, its contact time with the fractured bedrock surface is potentially larger than for melt water originating closer to the glacier snout. In these regions of the glacier, a higher portion of the melt water runs off via the glacier surface and through a more developed channelized subglacial drainage system (Tranter *et al.*, 1996). However, this concept is based on strong generalized assumptions, especially as the geometry of the subglacial drainage system within the glacier is highly variable and no constrains, as to which areas below the glaciers of the study area groundwater recharge may occur, are available. Additionally, melt water from the glacial ice is available for groundwater recharge throughout the base of the temperate glaciers because of frictional heat and the conductive heat flux from the bedrock (Menzies, 1995). Therefore, the assumption of the equilibrium line as a limit for preferential groundwater recharge from the glaciers poses a strong constrain on the spatial distribution of the recharge in these regions. Furthermore, the high amount of predicted groundwater recharge in these small regions of the glaciers is striking (up to 40% of mean precipitation rate). Even though substantial recharge may occur along fractures (Lerner *et al.*, 1990) with considerable water intake rates (Rasmussen and Evans, 1993; Gleeson *et al.*, 2009), such localized high recharge rates in the upper regions of the glaciers seem less plausible. A comparable recharge flux, distributed over a wider area of the glaciated regions might be a better approximation of the groundwater recharge below the glaciated areas.

A second factor for the dominance of the localized high recharge areas in the glaciated regions lies in the strong contrast in recharge rates between these areas and the neighbouring steep bare rock slopes, where very little recharge is predicted by the hydrological model. According to Forster and Smith (1988b), recharge rates along the summits might reach $\leq 10\%$ of the precipitation rate. Although it is plausible that liquid precipitation will preferentially enter fast surface runoff along the steep slopes, melt water from the winter snow cover is an important potential recharge source at these altitudes. This has been described by Rodhe (1998) and Hansmann *et al.* (2011) as a very efficient input to groundwater recharge. Snow cover along the Saashörner for example is generally substantial and especially topographic depressions, in this case small kars at the foot of the steep rock faces, might serve as potential recharge areas (Lissey, 1968; Lerner *et al.*, 1990). These numerous small areas are however not distinguished in the hydrological model because of the resolution of the applied model grid. The previously mentioned considerations might thus lead to an overestimation of the contrast in recharge rates along the partly glaciated crests of the mountain ridges in the Rotondo area.

The spread of the encountered tritium data in the northern section of the gallery has been attributed to varying flow velocities (reflected by different tritium concentrations) within separate hydraulic features such as fractures and small scale faults. In this sense, the groundwater system might be viewed as an assemblage of discrete water parcels that move along defined flow paths (Gat, 1981). Similar observations were made by Fontes *et al.* (1981) in a comprehensive study in the Mont-Blanc tunnel. Even though the homogeneous continuum approach cannot reproduce the potential heterogeneity of velocities present in the granite body due to discrete small scale fractures and faults, a certain spread of deduced travel times for flow towards this northern tunnel section can also be observed in this approach (Table VII).

The tritium data at the southern end of the accessible part of the Bedretto Tunnel displays a similar discrepancy with regard to the recharge source as the data at the northern end of the gallery. Although the scenarios with a distributed recharge predict mainly glacial melt water as recharge source, the uniform recharge variants delineate the slopes of the Wittenwasserenstock and the Rotondo as main recharge sources with only a minor glacial component. In general, the findings from the analysis of the chemical and environmental isotope composition of the groundwater encountered along the Bedretto Tunnel are reproduced in the model simulations. In particular the analysis of the observed tritium data along the Bedretto Tunnel allows an evaluation of the plausibility of the different recharge conditions applied in the model simulation.

CONCLUSION

In this paper, we presented hydraulic measurements from a deep tunnel in fractured crystalline rocks of the Swiss Alps and used this data subsequently to constrain a regional groundwater flow model. One of the aims was to investigate the effects of controlling factors on the flow system such as recharge conditions and structural elements in model simulations. The results of these simulations were compared with the findings of a previous study, as part of which, the environmental isotope composition and the hydrochemistry of the groundwater was investigated.

In the framework of the chosen continuum approach, the numerical simulations were able to provide valuable insights with regard to the impact of the subsurface galleries on the natural flow field within the Rotondo area and increased our understanding of the most influential parameters affecting the position of the groundwater table in a high alpine catchment area.

The water table position was shown to be sensitive to even small changes in prescribed hydraulic conductivities, with changes in elevation of several hundred metres for modifications of hydraulic conductivity of less than one order of magnitude. The significant decline of the water table below the mountain ridges of up to 600 m observed in the simulations is enhanced by the presence of the subsurface galleries, which generally modify the natural flow field by enhancing natural head gradients or even causing a reversal of the regional head gradients. The presence of a higher conductive fault zone with a *k*-value contrast to the surrounding bedrock of 1:10 causes no significant impact on the regional groundwater table, but most importantly acts as fast flowpath for groundwater recharging in glaciated areas in the eastern part of the study area and discharging to the Bedretto Tunnel. The internal anisotropy ratio of the horizontal components of hydraulic conductivity within the fault zone is less important because of the overall sub-parallel orientation of the fault zone with the orientation of the major horizontal component of hydraulic conductivity within the adjacent granite. Calibrated *k*-values for the Rotondo granite in the order of 6.5×10^{-9} to 1.2×10^{-8} m/s lie in the range of reported equivalent *k*-values for Hercynian granites of the Central Alps (Loew *et al*., 1996; Masset and Loew, 2010).

Spatially distributed groundwater recharge rates significantly affect the head distribution within the research area when compared with simulations with uniform recharge estimates. High relief massifs are more sensitive to changes in the recharge rate with regard to the water table elevation.

Compared with the interpretations based on the analysis of environmental isotopes and hydrochemistry, the numerical simulations underline that the groundwater recharge to the Bedretto Tunnel is derived from within the granite body with a potentially minor recharge contribution from an isolated amphibolite wedge in the Leckihorn area towards the northern end of the gallery.

In the combined interpretation of environmental isotopes and hydrodynamical modelling, we found the tritium data a very useful tool in the delineation of groundwater recharge sources in this alpine region. The analysis has shown that while the fault zone section in the Bedretto Tunnel is recharged by the glaciated areas to the east of the gallery, the northern section of the tunnel receives mainly groundwater inflow recharged from recent precipitation with a major component of accumulated winter precipitation. In the comparison of these findings, we could show that the spatially distributed recharge rates extracted from the hydrological model overestimate the contribution of the glaciated areas in groundwater recharge to the northern part of the tunnel. This is linked to the simplified assumption made in the hydrological model concerning the spatial discretization of groundwater recharge in the glaciated areas. A more physical based model of the glaciated areas (e.g. Arnold *et al*. (1998), Richards *et al*. (1996)), especially of the melt water routing through the glacial body, would aid the better understanding of the spatial availability of potential groundwater recharge and thus lead to a better representation of these recharge sources within the numerical groundwater flow model.

ACKNOWLEDGEMENTS

Access to the Furka Tunnel and the Bedretto Tunnel as well as logistic help was kindly provided by the Furka-Oberalp-Bahn. Then, digital elevation map DHM25 of the research area was used with approval by the Bundesamt für Landestopographie, Wabern (CH; Reference: BA013094). This research was funded by the ETH research fund.

REFERENCES

Abbott MD, Lini A, Bierman PR. 2000. δ^{18}O And ^{3}H measurements constrain groundwater recharge patterns in an upland fractured bedrock aquifer, Vermont, USA. *Journal of Hydrology* **228**: 101–112.

Abelin H, Birgersson L., Moreno L, Widen H, Agren T, Neretnieks I. 1991. A large-scale flow and tracer experiment in granite - 2. Results and interpretation. *Water Resources Research* **27**: 3119–3135.

Andersson J, Ekman L, Nordqvist R, Winberg A. 1991. Hydraulic testing and modelling of a low-angle fracture zone at Finnsjoen, Sweden. *Journal of Hydrology* **126**: 45–77.

Arnold N, Richards K, Willis I, Sharp M. 1998. Initial results from a distributed, physically based model of glacier hydrology. *Hydrological Processes* **12**: 191–219.

Badoux A. 1999. Untersuchung zur Flaechendifferenzierten Modellierung von Abfluss und Schmelze in teilvergletscherten Einzugsgebieten. MSc Thesis, Swiss Federal Institute of Technology (ETH) Zurich, Switzerland.

Balek J. 1988. Groundwater recharge concepts. In *Estimation of Natural Groundwater Recharge*, Simmers I (ed). NATO ASI Series. Series C **222**. D Reidel Publishing Company: Dordrecht; 3–11.

Bear J. 1993. Modeling flow and contaminant transport in fractured rocks. In *Flow and Contaminant Transport in Fractured Rock*, Bear J, Tsang C, de Marsily G (eds). Academic Press: Amsterdam; 1–38.

Brace WF. 1980. Permeability of crystalline and argillaceous rocks. *International Journal of Rock Mechnics & Mining Science* **17**: 241–251.

Brace WF. 1984. Permeability of crystalline rocks: new in situ measurements. *Journal of Geophyscial Research* **89**: 4327–4330.

Cacas MC, Ledoux E, De Marsily G, Barbreau A, Calmels P, Gaillard B, Margritta R. 1990a. Modeling fracture flow with a stochastic discrete fracture network: calibration and validation - 2. The transport model. *Water Resources Research* **26**: 491–500.

Cacas MC, Ledoux E, de Marsily G, Tillie B, Barbreau A, Calmels P, Gaillard B, Margrita R, Durand E, Feuga B, Peaudecerf P. 1990b. Flow and transport in fractured rocks: an in situ experiment in the Fanay-Augeres mine and its interpretation with a discrete fracture network model. *In Memoires of the 22nd Congress IAH*, Vol **XXII**. Lausanne; 13–37.

Cacas MC, Ledoux E, De Marsily G, Tillie B, Barbreau A, Durand E, Feuga B, Peaudecerf P. 1990c. Modeling fracture flow with a stochastic discrete fracture network: calibration and validation - 1. The flow model. *Water Resources Research* **26**: 479–489.

Caine JS, Forster CB. 1999. Fault zone architecture and fluid flow: insights from field data and numerical modeling. In *Faults and Subsurface Fluid Flow in the Shallow Crust*, Haneberg WC, Mozley PS, Moore JC, Goodwin LB (eds). American Geophysical Union: Washington D.C.; 101–127.

Caine JS, Evans JP, Forster CB. 1996. Fault zone architecture and permeability structure. *Geology* **24**: 1025–1028.

Carrera J, Heredia J. 1987. Inverse problem of chalk river block, HYDROCOIN level 2 (Case3) and level 2 (Case5a). *Technical Report NTB-88-14*. NAGRA.

Carrera J, Heredia J, Vomvoris S, Hufschmied P. 1990. Fracture flow modelling: application of automatic calibration techniques to a small fractured monzonitic gneiss block. In *Hydrogeology of Low Permeability Environments*, Neuman SP, Neretnieks I (eds). IAH - Selected Papers, Verlag Heinz Heise: Hannover (Germany); 115–167.

Clark ID, Fritz P. 1997. *Environmental Isotopes in Hydrogeology*. Lewis Publishers: Boca Raton, Florida.

Clauser C. 1992. Permeability of crystalline rocks. *Eos* **73**: 233–240.

Colenco. 1993. Gotthard-Basistunnel: Quantitative Analyse Hydrogeologischer Aufnahmen von Stollen- und Tunnelbauten im Gebiet Aar-Massiv-Gotthard-Massiv-Leventina. *Technical Report 1763/5*. Colenco Power Consulting.

Cruchet M. 1985. Influence de la decompression sur le comportement hydrogeologique des massifs cristallins En basse Maurienne (savoie, France). *Geologie Alpine* **61**: 65–73.

Davison CC, Kozak ET. 1988. Hydrogeologic characteristics of major fracture zones in a large granite batholith of the Canadian shield. In *Proceedings of the 4th {Canadian/American} Conference on Hydrogeology*. National Ground Water Association. Dublin, Ohio.

Davy P, Bour O, De-Dreuzy J-R, Darcel C. 2006. Flow in multiscale fractal fracture networks. In *Fractal Analysis for Natural Hazards*, vol. **261**, Cello G, Mulamud BD (eds). Geological Society: London. Special Publication; 31–45.

Diersch H-JG. 1998. *FEFLOW - Interactive, Graphics-Based Finite Element Simulation System for Modeling Groundwater Flow, Contaminant Mass and Heat Transport Processes, User's Manual*. WASY: Berlin.

Dverstorp B, Andersson J. 1989. Application of the discrete fracture network concept with field data: possibilities of model calibration and validation. *Water Resources Research* **25**: 540–50.

Evans JP, Forster CB, Goddard JV. 1997. Permeability of fault-related rocks, and implications for hydraulic structure of fault zones. *Journal of Structural Geology* **19**: 1393–404.

Flerchinger GN, Cooley KR, Ralston DR. 1992. Groundwater response to snowmelt in a mountainous watershed. *Journal of Hydology* **133**: 293–311.

Fontes JC, Bortolami GC, Zuppi GM. 1981. Hydrologie Isotopique Du Massif Du Mont-Blanc. In *Isotope Hydrology*. IAEA/UNESCO. Proceedings Symposium Neuherberg **1**, Vienna; 411–440.

Forster CB, Evans JP. 1991. Hydrology of thrust faults and crystalline thrust sheets: results of combined field and modeling studies. *Geophysical Research Letters* **18**: 979–982.

Forster C, Smith L. 1988a. Groundwater flow systems in mountainous terrain - 1. Numerical modeling technique. *Water Resources Research* **24**: 999–1010.

Forster C, Smith L. 1988b. Groundwater flow systems in mountainous terrain - 2. Controlling factors. *Water Resources Research* **24**: 1011–1023.

Forster CB, Goddard JV, Evans JP. 1994. Permeability structure of a thrust fault. In *Technical Report Open-File-Report 94–228. Proceedings of Workshop LXIII - The Mechanical Involvement of Fluids in Faulting*. USGS.

Frick U. 1994. The Grimsel radionuclide migration experiment - a contribution to raising confidence in the validity of solute transport models used in performance assessment. In *GEOVAL '94 - Validation throgh Model Testing, Proceedings of an NEA/SKI Symposium*. OECD Nuclear Energy Agency; 245–273.

Gat JR. 1981. Groundwater. In *Stable Isotope Hydrology. Deuterium and Oxygen-18 in the Water Cycle*, Gat JR, Gonfiantini R (eds). IAEA: Vienna; 223–240.

Gleeson T, Manning AH. 2008. Regional groundwater flow in mountainous terrain: three-dimensional simulations of topographic and hydrogeologic control. *Water Resources Research* **44**: W10403.

Gleeson T, Novakowski K, Kyser TK. 2009. Extremely rapid and localized recharge to a fractured rock aquifer. *Journal of Hydrology* **376**: 496–509.

Goodman RE. 1965. Ground water inflows during tunnel driving. *Engineering Geology* **2**: 39–56.

Guimera J, Carrera J. 1997. On the interdependence of transport and hydraulic parameters in Low permeability fractured media. In *Hard Rock Hydrosystems*, Pointet T (ed). IAHS Publication No. 241, IAHS Press: Wallingford (UK); 123–133.

Gurtz J, Peschke G, Mendel O. 1990. Hydrologic processes in small experimental areas influenced by vegetation cover. In H*ydrological Research Basins and Environment Proceedings and Information No. 44*. International Conference Wageningen; 61–69.

Gurtz J, Baltensweiler A, Lang H. 1999. Spatially distributed hydrotope-based modelling of evapotranspiration and runoff in mountainous basins. *Hydrological Processes* **13**: 2751–2768.

Hansmann J, Loew S, Evans KF. 2011. Reversible rock-slope deformations caused by cyclic water table fluctuations in mountain slopes of the Central Alps, Switzerland. *Hydrogeology Journal* **20**: 73–91.

Heppner C, Nimmo J, Folmar G, Gburek W, Risser D. 2007. Multiple-methods investigation of recharge at a humid-region fractured rock site. *Hydrogeology Journal* **15**: 915–927.

Herbert A, Gale J, Lanyon G, MacLeod R. 1991. Modelling for the stripa site characterization and validation drift - inflow: prediction of flow through fractured rock. *Technical Report SKB91-35*. SKB.

Himmelsbach T, Hoetzl H, Maloszewski P. 1998. Solute transport processes in a highly permeable fault zone of Lindau fractured rock test site. *Ground Water* **36**: 792–800.

Hsieh PA, Neuman SP, Stiles GK, Simpson ES. 1985. Field determination of the three-dimensional hydraulic conductivity tensor of anisotropic media - 2. Methodology and application to fractured rocks. *Water Resources Research* **21**: 1667–1676.

ISO. 1997. Measurement of liquid flow in open channels - velocity-area methods. *Technical Report ISO 748:1997(E)*. International Organization for Standardisation, Geneva.

Jamier D. 1975. Etude de la Fissuration, de L'hydrogeologie et de la Geochemie Des Eaux Profondes Des Massifs de L'arpille et Du Mont-Blanc. PhD Thesis, Faculte des Sciences de l'Universite de Neuchatel, Switzerland.

Kattelmann R, Elder K. 1991. Hydrologic characteristics and water balance of an alpine basin in the Sierra Nevada. *Water Resources Research* **27**: 1553–1562.

Keller F, Schneider TR. 1982. Der Furka-Basistunnel - Zur Eroeffnung am 25. Juni 1982; Geologie und Geotechnik. *Schweizer Ingenieur und Architekt* **24**: 512–520.

Kimmermeier E, Perrochet P, Andrews R, Kiraly L. 1985. Simulation par Modele Mathematique des Ecoulements Souterrains Entre Les Alpes et la Foret Noire. Technical Report NTB-84-50. NAGRA.

Kitterod N, Colleuille H, Wong WK, Pedersen TS. 2000. Simulation of groundwater drainage into a tunnel in fractured rock and numerical analysis of leakage remediation, Romeriksporten tunnel, Norway. *Hydrogeology Journal* **8**: 480–93.

Koella E. 1993. Gotthard-Basistunnel - Regional Hydrogeologie im Projektgebiet unter Besonderer Berueckichtigung des Ritom-Gebietes. Unpublished Report from 30.11.1993.

Labhart TP. 1999. Aarmassiv, Gotthardmassiv und Tavetscher Zwischenmassiv: Aufbau und Entstehungsgeschichte. In *Vorerkundung und Prognose des Basistunnel am Gotthard und am Loetschberg Proceedings Symposium Geologie Alptransit*. Loew S, Wyss R (eds). A.A. Balkema: Rotterdam (NL); 31–43.

Legchenko A, Beauce A, Ofterdinger US, Renard P. 1998. Field tests of the surface proton magnetic resonance instrument NUMIS in fractured crystalline rocks of the Western Gotthard-Massif (Switzerland). Technical Report BRGM-ETH3465/13. Department of Geology, Swiss Federal Institute of Technology (ETH) Zurich, Switzerland.

Lerner DN, Issar AS, Simmers I. 1990. *Groundwater Recharge – A Giude to Understanding and Estimating Natural Recharge*. Heinz Heise: Verlag.

Lissey A. 1968. Surficial mapping of groundwater flow systems with application to the Oak River Basin, Manitoba. PhD Thesis, University of Saskatchewan.

Loew S, Ehrminger B, Klemenz W, Gilby D. 1996. Abschaetzung von Bergwasserzufluessen und Oberflaechenauswirkungen am Beispiel des Gotthard-Basistunnels. In *Instabile Haenge und andere Risikorelevante Natuerliche Prozesse*, Oddsson B (ed). Birkhaeuser: Verlag; 353–376.

Loew S, Ziegler H, Keller F. 2000. AlpTransit: engineering geology of the world's longest tunnel system. In *GeoEng2000-International Conference on geotechnical and Geological Engineering, Melbourne*. Technomic Publishing Co.: Lancaster, PA; 927–37.

Loew S, Luetzenkirchen VH, Ofterdinger U, Zangerl C, Eberhardt E, Evans K. 2007. Environmental impacts of tunnels in fractured crystalline rocks of the Central Alps. In *Groundwater in Fractured Rocks – IAH-Selected Papers 9*, Krasny J, Sharp JM (eds). Taylor & Francis: London; 55–68.

Long JCS, Remer JS, Wilson CR, Witherspoon PA. 1982. Porous media equivalents for networks of discontinuous fractures. *Water Resources Research* **18**: 645–658.

Lopez DL, Smith L. 1995. Fluid flow in fault zones: analysis of the interplay of convective circulation and topographically driven groundwater flow. *Water Resources Research* **31**: 1489–1503.

Lopez DL, Smith L. 1996. Fluid flow in fault zones: influence of hydraulic anisotropy and heterogeneity on the fluid flow and heat transfer regime. *Water Resources Research* **32**: 3227–3235.

Luetzenkirchen VH. 2002. Structural geology and hydrogeology of brittle fault zones in the central and eastern Gotthard massif. PhD thesis, Swiss Federal Institute of Technology (ETH) Zurich, Switzerland.

Luetzenkirchen VH, Loew S. 2001. Regional ground water flow in cataclastic fault zones. Results from large scale tracer test in the Swiss Alps. In *Proceedings XXXI Congress IAH*. Seiler K-P (ed). Munich.

Luetzenkirchen VH, Loew S. 2011. Late alpine brittle faulting in the rotondo granite (Switzerland): deformation mechanisms and fault evolution. *Swiss Journal of Geosciences* **104**: 31–54.

Manning AH, Caine JS. 2007. Groundwater noble gas, age, and temperature signatures in an alpine watershed: valuable tools in conceptual model development. *Water Resources Research* **43**: W04404.

Manning AH, Solomon DK. 2005. An integrated environmental tracer approach to characterizing groundwater circulation in a mountain block. *Water Resources Research* **41**: W12412.

Marechal JC. 1998. Les circulations d'eau dans les massifs cristallins alpins et leurs relations avec les ouvrages souterrains. PhD thesis, Ecole Polytechnique Federale de Lausanne.

Marechal JC. 2012. Les Tunnels Alpins: Observatoires de L'Hydrogeologie des Grands Massifs Montagneux. *La Houille Blanche* **1**: 44–50.

Marechal JC, Etcheverry D. 2003. The use of ^{3}H and ^{18}O tracers to characterize water inflows in Alpine Tunnels. *Applied Geochemistry* **18**: 339–351.

Martinec J, Oeschger H, Schotterer U, Siegenthaler U. 1982. Snowmelt and groundwater storage in an Alpine Basin. In *Hydrological Aspects of Alpine and High Mountain Areas*. Glenn JW (ed). IAHS Publication No. 138: Birmingham (UK); 169–175.

Masset O. 2011. Transient tunnel inflow and hydraulic conductivity of fractured crystalline rocks in the Central Alps (Switzerland). PhD Thesis, Swiss Federal Institute of Technology (ETH) Zurich, Switzerland.

Masset O, Loew S. 2010. Hydraulic conductivity distribution in crystalline rocks, derived from inflows to tunnels and galleries in the Central Alps, Switzerland. *Hydrogeology Journal* **18**: 863–891.

Menzies J. 1995. Hydrology of glaciers. In *Modern Glacial Environments*, Menzies J (ed). Butterworth-Heinemann: Oxford; 197–240.

Nagra. 1988. Berichterstattung ueber die Untersuchungen der Phase I Am Potentiellen Standort Piz Pian Grand (Gemeinden Mesocco und Rossa, GR). Technical Report NTB88-19. Nagra.

Neretnieks I. 1983. A note on fracture flow mechanisms in the ground. *Water Resources Research* **19**: 364–370.

Neretnieks I. 1993. Solute transport in fractured rock - applications to radionuclide waste repositories. In *Flow and Contaminant Transport in Fractured Rock*, Bear J, Tsang C, de Marsily G (eds). Academic Press: Amsterdam; 39–128.

NRC. 1996. *Rock Fractures and Fluid Flow*. National Research Council (NRC), National Academic Press: Washington D.C.

Ofterdinger US. 2001. Groundwater flow systems in the Rotondo Granite, Central Alps (Switzerland). PhD thesis, Swiss Federal Institute of Technology (ETH) Zurich, Switzerland.

Ofterdinger US, Balderer W, Loew S, Renard P. 2004. Environmental isotopes as indicators for ground water recharge to fractured granite. *Ground Water* **42**: 868–879.

Priest SD. 1993. *Discontinuity Analysis for Rock Engineering*. Chapman and Hall: London.

Rasmussen TC, Evans DP. 1993. Water infiltration into exposed fractured rock surfaces. *Soil Science Society Journal* **57**: 324–329.

Raven K.G. 1977. Preliminary evaluation of structural and groundwater conditions in underground mines and excavations. In *Report of Activities*. Geological Survey of Canada; 39–42.

Raven KG. 1985. Field investigations of a small ground water flow system in fractured monzonitic gneiss. In *Hydrogeology of Rocks of Low Permeability-Proceedings 17th International Congress {IAH}*. IAH; 72–86.

Richards K, Sharp M, Arnold N, Gurnell A, Clark M, Tranter M, Nienow P, Brown G, Willis I, Lawson W. 1996. An integrated approach to modelling hydrology and water quality in glacierized catchments. *Hydrological Processes* **10**: 479–508.

Rodhe A. 1998. Snowmelt-dominated systems. In *Isotope Tracers in Catchment Hydrology*, Kendall C, McDonnell JJ (eds). Elsevier: Amsterdam; 391–433.

Scanlon B, Healy R, Cook P. 2002. Choosing appropriate techniques for quantifying groundwater recharge. *Hydrogeology Journal* **10**: 18–39.

Schneider TR. 1976. Furka-Basistunnel – Zur Frage Von Stoerungen im Bereich des Fensterpunktes des Bahntunnels. *Technical Report 338 h*. Furka-Oberalp-Bahn. Brig (CH).

Schneider TR. 1985a. Basistunnel-Furka, Los 63-Bedretto, Geologische Aufnahme des Fensters. *Technical Report 338 g*. Furka-Oberalp-Bahn. Brig (CH).

Schneider TR. 1985b. Geologischer Schlussbericht, Furka-Basistunnel. *Technical Report 338o*. Furka-Oberalp-Bahn. Brig (CH).

Scholz CH, Anders MH. 1994. The permeability of faults. In *Technical Report Open-File-Report 94–228 Proceedings of Workshop LXIII- The mechanical involvement of fluids in faulting*. USGS.

Smith L, Clemo T, Robertson MD. 1990a. New approaches to the simulation of field-scale solute transport in fractured rocks. In *Proceedings 5th Canadian/American Conference on Hydrogeology*, Bachu S (ed). National Well Association: Dublin, Ohio; 329–342.

Smith L, Forster C, Evans J. 1990b. Interaction of faultzones, fluid flow and heat transfer at the basin scale. In *Hydrogeology of Low Permeability Environments*, Neuman SP, Neretnieks I (eds). IAH - Selected Papers, Verlag Heinz Heise: Hannover (Germany); 41–67.

Snow DT. 1968. Rock fracture spacings, openings, and porosities. *Journal of the soil mechanics and foundation division, ASCE* **94**: 73–90.

Thury M, Gautschi A, Mazurek M, Mueller WH, Naef H, Pearson FJ, Vomvoris S, Wilson W. 1994. Geology and hydrogeology of the crystalline basement of Northern Switzerland. Technical Report NTB93-01. NAGRA.

Toth J. 1963. A theoretical analysis of groundwater flow in small drainage basins. *Journal of Geophysical Research* **68**: 4795–4812.

Toth J. 1984. The role of regional gravity flow in the chemical and thermal evolution of ground water. In Practical Applications of Ground Water Geochemistry Proceedings 1st Canadian/American Conference on Hydrogeology. Hitchon B, El W. (eds). Worthington, Ohio. National Water Well Association and Alberta Research Council; 3–39.

Tranter M, Brown GH, Hodson AJ, Gurnell AM. 1996. Hydrochemistry as an indicator of subglacial drainage system structure: a comparison of Alpine and sub-polar environments. *Hydrological Processes* **10**: 541–556.

Vitvar T, Gurtz J. 1999. Spatially distributed hydrological modeling in the rotondo area, western gothard-massif. Technical Report 3465/16 Department of Geology Swiss Federal Institute of Technology (ETH) Zurich, Switzerland.

Viviroli D, Zappa M, Gurtz J, Weingartner R. 2009. An introduction to the hydrological modelling system PREVAH and its pre- and post-processing tools. *Environmental Modelling & Software* **24**: 1209–1222.

Voborny O, Adank P, Huerlimann W, Vomvoris S, Mishra S. 1991. Grimsel test site – modeling of groundwater flow in the rock body surrounding the underground laboratory. Technical Report NTB91-03. NAGRA.

Voborny OS, Vomvoris S, Wilson G, Resele G, Huerlimann W. 1994. Hydrodynamic synthesis and modeling of groundwater flow in crystaline rocks of Northern Switzerland. Techncial Report92-04. NAGRA.

Wallace RE, Morris HT. 1979. Characteristics of faults and shear zones as seen in mines at depths as much as 2.5 km below the surface. Technical Report Open-File-Report 79–1239. USGS.

Walton-Day K., Poeter E. 2009. Investigating hydraulic conenctions and the origin of water in a mine tunnel using stable isotopes and hydrographs. *Applied Geochemistry* **24**: 2266–2282.

Ward JV, Malard F, Tockner K, Uehlinger U. 1999. Influence of ground water on surface water conditions in a galcial flood plain of the Swiss Alps. *Hydrological Processes* **13**: 277–293.

Winkler G, Kurz W, Hergarten S, Kiechl E. 2010. Hydraulic characterization of core zones in crystalline hard rocks at teh talhof fault (Eastern Alps). *Grundwasser* **15**: 59–68.

Winter TC. 2001. The concept of hydrologic landscape. *Journal of the American Water Resources Association* **37**: 335–349.

Zangerl C, Loew S, Eberhardt E. 2006. Structure, geometry and formation of brittle discontinuities in anisotropic crystalline rocks of the Central Gotthard Massif, Switzerland. *Eclogae Geologicae Helvetiae* **99**: 271–290.

Zijl W. 1999. 1. *Hydrogeology Journal* **7**: 139–50.